Available online at www.sciencedirect.com
SCIENCE DIRECT®
Journal of volcanology and geothermal research
ELSEVIER
Journal of Volcanology and Geothermal Research xx (2006) xxx–xxx
www.elsevier.com/locate/jvolgeores

The volatile content of magmas from Arenal volcano, Costa Rica

Jennifer A. Wade [a,*], Terry Plank [a], William G. Melson [b], Gerardo J. Soto [c], Erik Hauri [d]

[a] Department of Earth Sciences, Boston University, Boston, MA 02215, USA
[b] Division of Petrology and Volcanology, National Museum of Natural History, Smithsonian Institution, Washington, DC 20560, USA
[c] Apdo. 360-2350 San Francisco de Dos Ríos, Costa Rica
[d] Department of Terrestrial Magnetism, Carnegie Institution of Washington, Washington, DC 20015, USA

Received 17 June 2005; accepted 28 March 2006

Abstract

We provide the first direct measurements of water in mafic melts from Arenal volcano, Costa Rica. Ion microprobe analyses of olivine-hosted melt inclusions (MI) from the prehistoric ET3 and ET6 tephra layers reveal high concentrations of volatile species: ~ 1–4 wt.% H_2O, 50–300 ppm CO_2, and >3000 ppm S and Cl. The MI with the highest water concentrations are the most mafic, and the dataset as a whole records a history of degassing coupled with fractionation and ascent from ~ 2 kbar to 0.2 kbar. Arenal MI form two groups based on their Al, CO_2 and S contents. The ET3 high-Al MI were trapped at the highest pressure, are closest to equilibrium with their host olivines (~ Fo_{79}), which are closest to equilibrium with the bulk-rock liquid. These MI are excellent candidates for Arenal parental liquids, and can generate most Arenal volcanic rock compositions by crystal accumulation (up to 30%), or crystal fractionation at a range of pressure (0.5–3 kb) and H_2O contents (0.5–3.5 wt.%). The new sulfur data reported here predict total sulfur output over the past ~ 30 years from bulk basaltic andesite liquid that matches well spectroscopic estimates, and resolves the previously noted imbalance. MI from different ET3 and ET6 samples show different F/Cl, while most trace element ratios show a limited range similar to that of the host rocks. The high water content (4 wt.% H_2O) of Arenal basaltic magma is somewhat surprising given the weak subduction signal recorded geochemically (e.g., low ^{10}Be and B). The Arenal MI data contribute to a positive correlation between primary water contents and Ba/La in Central American volcanoes, although further testing is required given the small number of data points, and the expectation that water and trace elements should have different sources in the subduction zone.

1. Introduction

Arenal volcano is a small (~ 15 km^3; Carr, 1984) and young (~ 7000 years, Soto et al., 1998; Soto and Alvarado, this issue) stratovolcano located in northwest Costa Rica. It falls in the center of the Costa Rican portion of the Central American volcanic front. Arenal's history has been dominated by four ~ 800-year-long cycles between subplinian eruptions, with strong strombolian and minor eruptions in between (Ghigliotti et al., 1993; Borgia et al., 1988; Soto et al., 1998).

The volcano's cyclic eruptive history has been recorded in a layered stratigraphy that has been well-studied, particularly since the onset of the current, steady-state andesitic eruption in 1968 (Melson and Saenz, 1973; Melson, 1983; Reagan et al., 1987; Borgia et al., 1988; Beard and Borgia, 1989; Cigolini, 1998; Streck et al., 2002, 2005, and manuscripts from this issue). Petrological models for the evolution of Arenal magmas place different emphasis on the importance of crystal fractionation,

* Corresponding author. Tel.: +1 617 353 4085; fax: +1 617 353 3290.
E-mail address: jwade@bu.edu (J.A. Wade).

0377-0273/$ - see front matter © 2006 Published by Elsevier B.V.
doi:10.1016/j.jvolgeores.2006.03.045

Fig. 1. Map of Central America, with arc-front volcanoes as triangles.

magma mixing, crystal accumulation, and entrainment of xenoliths and xenocrysts of different compositions. A common theme, however, is the continuous supply to the Arenal system of mafic precursor magma. This often "unseen" parent magma is inferred to have high water contents (≥3 wt.%), manifest in eruptives with high Al concentrations, high An plagioclase, and most significantly, hornblende (Reagan et al., 1987; Borgia et al., 1988). This view of a prevalent, parental magma with high initial water contents runs counter to geochemical evidence that Arenal magmas have a weak 'subduction signal,' with low values of various slab tracers (e.g., ^{10}Be, Tera et al., 1986; B/La, Leeman et al., 1994). Resolving this apparent contradiction requires direct measurements of the water content of Arenal magmas, which is the purpose of this study.

Water plays a vital role in subduction zones. Originally present in slab sediments and hydrous minerals of the subducting lithosphere, and later released in dehydration and melting reactions, water drives mantle melting, and influences crystal fractionation and eruption style (Sisson and Grove, 1993; Stolper and Newman, 1994; Roggensack et al., 1997). Despite its central role in these processes, few quantitative measurements of H_2O have been made in arc volcanoes, as all magma degasses upon ascent and eruption. Rare olivines, however, may trap melt at depths greater than H_2O-vapor saturation and the analysis of such melt inclusions may thus permit robust estimates of the initial H_2O content of arc magmas (Anderson, 1979; Sisson and Layne, 1993).

Central America is a good place to look for variations in magmatic water content because other tracers from the slab, such as ^{10}Be, Ba/La, and U/Th show systematic variations along strike, peaking in Nicaragua and descending to the northwest into Guatemala, and southeast into Costa Rica (Carr et al., 1990; Leeman et al., 1994; Patino et al., 2000). Water concentration has been measured in olivine-hosted melt inclusions in a few volcanoes along the Central American arc. Cerro Negro in Nicaragua lies near the geographical peak in slab tracers (including ^{10}Be and Ba/La), and basaltic melt inclusions contain, on average, ~ 5 wt.% H_2O (Roggensack et al., 1997, 2001a, b). To the northwest in Guatemala and southeast in Costa Rica, where Ba/La is generally much lower, magmatic water contents are also lower (~ 2 wt.% at Pacaya and ~ 4 wt.% at Fuego; Walker et al., 2003 and ~ 3% at Irazú; Benjamin et al., 2004). Still it is unclear whether or not "slab tracers" like Ba/La are directly related to H_2O contents. Specifically, are the sources of Ba and Be (and the means by which they are transported from the slab) the same as those which deliver H_2O?

We have made the first direct measurements of H_2O, in addition to several other volatile species (e.g. CO_2, S, Cl, F) dissolved in olivine-hosted melt inclusions from Arenal tephra, in order to better constrain the nature of the parent magma, as well as to evaluate whether or not traditional "slab tracers" are accurate fluid proxies. Both geographically and geochemically, Arenal falls in the middle, between Cerro Negro's wet, high-slab signal and Irazú's low slab signal near the southeast terminus of the Central American volcanic arc (Fig. 1).

2. Background

2.1. Eruptive history of Arenal

Arenal awoke from its most recent period of quiescence (since ~ 1700 AD) in July, 1968 and continues to

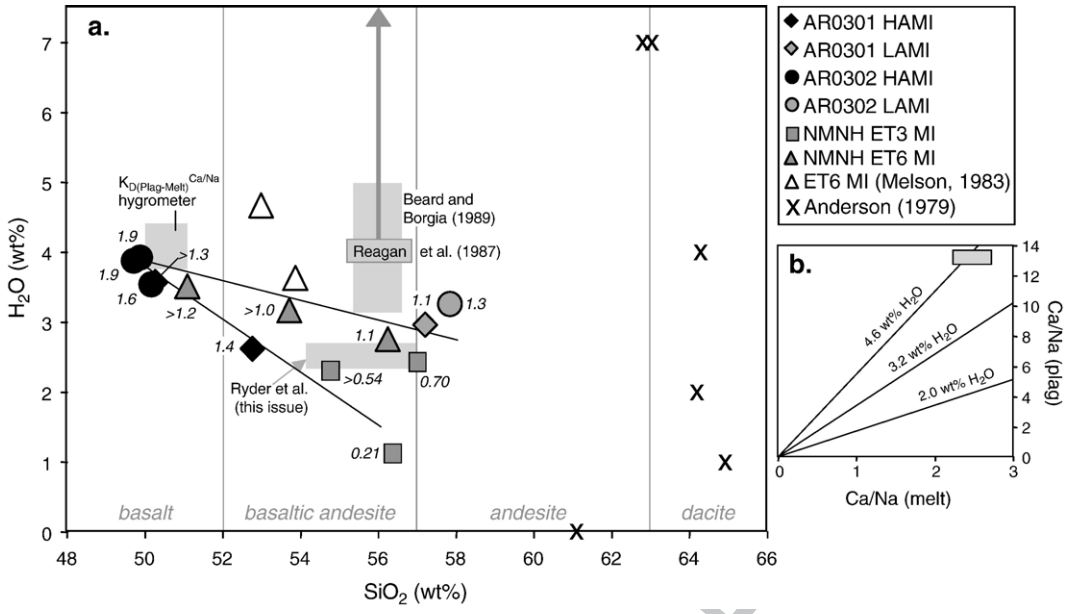

Fig. 2. a) Summary of previous H_2O estimates for Arenal compositions, plus new melt inclusion data in ET3 and ET6 olivines. Reagan et al. (1987) estimate >4% H_2O based on the presence of hornblende and An_{94} plagioclase in the early phases of the current eruption, requiring pH_2O up to 5 kbar. Estimate from Beard and Borgia (1989) is also based on the presence of hornblende. The estimate by Ryder et al. (2005) is derived from MELTS modeling. Data points are olivine-hosted melt inclusions from this study (Table 1) and plag-, cpx-, and magnetite-hosted melt inclusions from Anderson (1979). Open NMNH ET6 points are original sum–deficit estimate from Melson (1983). Values adjacent to data points indicate H_2O–CO_2 vapor saturation pressures from Fig. 9. b) Plagioclase–melt Ca/Na exchange hygrometer from Sisson and Grove (1993). Lines of constant water represent $K_D^{Ca/Na}{}_{(plag-melt)}$ of 5.5 (2 kbar H_2O-saturated), K_D=3.4 (1 kbar H_2O-saturated), and K_D=1.7 (2 wt.% H_2O). Ca/Na ratios are molar. H_2O saturation at 1 and 2 kbar revised from values given by Sisson and Grove (1993) to be consistent with the solubility model in Newman and Lowenstern (2002) used in this study (e.g. see Fig. 9). Plag Ca/Na is based on maximum An (92.8–93.1) measured in basal ET3 units (Bolge et al., 2004).

erupt as of this writing. Borgia et al. (1988) describe the stratigraphy based on alumina content within each of the four eruptive cycles in Arenal's past, composed of a high alumina group (HAG, >20% Al_2O_3), low alumina group (LAG), an intermediate group, and finally the dacitic and basaltic tephras, two of which are discussed in detail in this text (tephra units ET3 and ET6, originally described by Melson, 1983). In their model, an 'unseen' basaltic magma evolves early, and through fractionation and the redistribution of phases, generates a zoned andesite body, which then evolves into an andesite/dacite cap. Throughout this period of zonation and fractionation, the mafic, parent magma may be mixing with its own products (such as plagioclase or gabbroic cumulates) or entraining crustal xenoliths (Cigolini, 1998). When this zoned magma body erupts, it generates the Al-zoned stratigraphy observed on the slopes of Arenal today. Based on the observance of hornblende solely in material from the first blasts of the current eruption (Reagan et al., 1987; Borgia et al., 1988), this model proposes that the beginning of each eruptive phase is marked by high-pH_2O, which decreases over the course of the cycle.

2.2. Previous H_2O estimates from Arenal eruptives

The first estimates of water concentration in Arenal magmas were made using the difference from 100% of major element analyses by electron microprobe (sum–deficit technique). Anderson (1979) studied lapilli from the earliest blast of the 1968 eruption. The recent eruption is olivine-poor, and the only inclusions available were plagioclase-, pyroxene-, and magnetite-hosted andesite–dacite melts, which yielded H_2O contents of 0–7 wt.% (Fig. 2a). The inclusions with the lowest water concentration are most likely degassed, but if Arenal magmas do indeed contain up to 7% H_2O, these would be the highest-water contents measured in mafic Central American magmas. Sum–deficit H_2O estimates of 3.6 and 4.5 wt.% were made by Melson (1983; Fig. 2a) in 2 basaltic–andesite melt inclusions in one olivine (Fo_{75}) from a prehistoric tephra, ET6 (recently re-named AR-16 by Soto and Alvarado, this issue). Such high water contents are not surprising considering the units were explosive. Melson (1983)'s estimate of the H_2O content in ET6 is the estimate most widely used as representative of the Arenal mafic parent.

Other estimates of magmatic water contents at Arenal are more indirect. Borgia et al. (1988) suggest that a buildup of pH_2O (leading to variable H_2O contents) in the pre-eruptive body beneath Arenal might contribute to the volcano's cyclic explosivity. Streck et al. (2005) suggest a correlation between high An plagioclase and deep, continuously-replenishing high-H_2O source magmas. Reagan et al. (1987) note that hornblende is present in materials ejected during the early, explosive stages of the current eruption, but then disappears, indicating high pH_2O conditions (4–9 wt.% H_2O, although they ultimately preferred the lower end of that range) (Fig. 2a). Beard and Borgia (1989) also use the presence of hornblende in gabbroic enclaves to indicate 3–5% H_2O in Arenal basaltic andesites.

In summary, previous estimates support a water-rich magma parental to Arenal, but considerable uncertainty exists as to actual H_2O abundances. Sum–deficit measurements can yield useful estimates of water concentration (within 1% of measured values; Sisson and Layne, 1993), but pitfalls in microprobe analyses can lead to low sums. The stability of amphibole is dependent on several parameters, including temperature, pressure, and Na content (Sisson and Grove, 1993), in addition to water. Our goal is thus to make the first direct measurements of water and other volatile species in Arenal magmas, in order to constrain primary volatile compositions and test existing petrologic models.

2.3. Explosive tephra units ET3 and ET6

As the first formed mineral in a mafic magma, olivine is the most likely to trap primitive melt at high pressures, before the magma has substantially degassed its water. Olivines found in lapilli tephra, rather than lavas, are strongly preferred, as the inclusions within them cool quickly, minimizing loss of H out of the olivine by diffusion or through cracks (Hauri, 2002). Lapilli < 3 cm further minimizes post-entrapment effects such as crystallization of the glass, or reaction between the melt and the host grain (Luhr, 2001). We have therefore focused our sampling on two of the most mafic tephra units in Arenal's eruptive history: ET3 (deposited ~ 930 BP) and ET6 (deposited ~ 1250 BP; Soto and Alvarado, 2005). The new nomenclature in Soto and Alvarado (this issue) redefines ET3 as AR-19 and ET6 as AR-16, but we retain here the original ET sample names to prevent confusion with the previous work cited within this study. These units were first described by Melson (1983) at 'El Tajo' (a former quarry west of the volcano, presently under the water of Arenal reservoir). ET3 and ET6 mark the mafic eruptions that end two of the four 800-year-long eruptive cycles in Arenal's history (Melson and Saenz, 1973; Melson, 1983; Borgia et al., 1988; Soto et al., 1998). These prehistoric units contrast with materials from the current 'andesitic steady-state eruption' in which olivine is exceedingly rare (Reagan et al., 1987; Streck et al., 2005).

Tephra from the ET3 and ET6 units are very similar to each other in composition, although ET3, which belongs to the HAG of Borgia et al. (1988) is higher in Al and Na, and contains fewer plagioclase phenocrysts than ET6 (part of the LAG; Borgia et al., 1988). Stratigraphically, ET3 is much thicker and more voluminous than ET6, although erosion during the repose period after deposition of each may have obscured their true eruptive volumes (Melson, 1983; Soto et al., 2000). Both deposits (ET6 and ET3) are characterized by several layers of coarse, black lapilli separated by fine lapilli, ashes, and accretionary lapilli, which most likely indicate repeated explosive events, probably separated by short repose periods marked by unconformities, as can be seen in the most proximal sections of ET3 (Melson, 1983; Soto et al., 1998, 2000). Compositional variations with the ET3 unit are systematic with stratigraphic level, and record decreasing crystal accumulation towards the top (Bolge et al., 2004).

Two new samples of lapilli from ET3 (AR0301 and AR0302; Table 1) were collected in January, 2003 from a roadcut along the Entrance to Mirador El Silencio, between La Fortuna and Sangregado Dam (UTM coordinates: $^{4}56^{150}$ m.E, $^{2}74^{080}$m.N). These samples both yielded olivine-hosted melt inclusions, and are the primary focus of this study. Sample AR0302 was taken immediately above ET4, and represents the basal deposit and thus the first tephra of the ET3 eruption. AR0301 was collected 20 cm above AR0302. The dominant phenocryst in AR0301 is plagioclase, and grains are fairly uniformly-sized. This vesicular sample also contains clinopyroxene and minor olivine. The dominant phenocryst in AR0302 is also plagioclase, with larger populations of clinopyroxene and olivine than AR0301. AR0302 is much coarser-grained and less vesicular than AR0301. We also analyzed olivine-hosted melt inclusions in thin sections from the ET3 and ET6 samples originally described by Melson et al. (1983) from the type El Tajo section. These samples are indicated by their National Museum of Natural History (NMNH) sample number (Table 1).

3. Analytical methods

Each hand sample was brushed, rinsed with MilliQ water to remove surface impurities, and dried. Visibly unweathered sections were cut from each sample, and a portion was powdered for bulk-rock analysis while the

t1.1 Table 1
t1.2 Major element and volatile analyses of melt inclusions

t1.3 Unit	ET3	ET3	ET3	ET3	ET3	ET3	ET3
t1.4 Sample name	AR0301-1a	AR0301-2a	AR0301-3b	AR0301-13a	AR0301-13b	AR0302-1a	AR0302-1b
t1.5 Notes	LAMI	HAMI	HAMI	HAMI	HAMI	HAMI	HAMI
t1.6 SiO_2	57.42	53.23	51.73	*50.29*	*51.97*	49.71	50.60
t1.7 TiO_2	1.68	0.85	2.77	*0.82*	*1.36*	0.70	0.57
t1.8 Al_2O_3	15.64	18.40	19.90	*18.83*	*18.15*	17.92	19.08
t1.9 FeO	6.07	7.90	5.41	*7.36*	*6.67*	7.79	6.51
t1.10 Fe_2O_3	1.69	2.19	1.50	*2.04*	*1.85*	2.16	1.81
t1.11 MnO	0.12	0.23	0.16	*0.20*	*0.30*	0.22	0.17
t1.12 MgO	3.02	3.24	2.74	*4.76*	*3.97*	4.18	2.21
t1.13 CaO	5.88	8.02	10.80	*9.56*	*7.51*	9.20	9.64
t1.14 Na_2O	2.30	2.56	2.53	*3.14*	*4.15*	2.53	2.84
t1.15 K_2O	0.60	0.45	0.32	*0.63*	*0.73*	0.46	0.50
t1.16 P_2O_5	*0.27*	*0.17*		*0.20*	*0.19*	0.16	0.13
t1.17 Total	94.7	97.3	97.9	97.8	96.8	95.0	94.1
t1.18 Mg#	47.0	42.3	47.4	53.5	51.5	48.9	37.7
t1.19 H_2O (wt.%)	2.95	2.61		3.56		3.88	3.93
t1.20 CO_2 (ppm)	118	310		c.c		170	179
t1.21 F (ppm)	649	610		576		315	326
t1.22 S (ppm)[1]	1070	2000		2480		2170	2770
t1.23 S (ppm)[2]	1060	1970	2300			1980	2190
t1.24 S (ppm)[3]	887	1790		3020	3400		
t1.25 % SO_4 of total sulfate	84%	84%		78%			
t1.26 Log fO_2 (ΔNNO)	+1.10	+1.10		+0.93			
t1.27 Cl (ppm)[1]	2920	1540		1290		1490	1740
t1.28 Cl (ppm)[2]	2790	1320	1100			1780	1970
t1.29 Cl (ppm)[3]	2550	1540		1280	1720		
t1.30							
t1.31 *Host-corrected compositions*							
t1.32 Olivine added	1%	3%	3%	0%	0%	0%	6%
t1.33 SiO_2	57.23	52.78	51.35	*50.29*	*51.97*	49.71	49.88
t1.34 TiO_2	1.68	0.83	2.77	*0.82*	*1.36*	0.70	0.54
t1.35 Al_2O_3	15.49	17.86	19.32	*18.83*	*18.15*	17.92	18.00
t1.36 FeO	6.24	8.4	5.89	*7.36*	*6.67*	7.8	7.61
t1.37 Fe_2O_3	1.67	2.1	1.46	*2.04*	*1.85*	2.2	1.70
t1.38 MnO	0.12	0.22	0.16	*0.20*	*0.30*	0.22	0.16
t1.39 MgO	3.37	4.22	3.81	*4.76*	*3.97*	4.18	4.14
t1.40 CaO	5.82	7.79	10.49	*9.56*	*7.51*	9.20	9.09
t1.41 Na_2O	2.28	2.49	2.46	*3.14*	*4.15*	2.53	2.68
t1.42 K_2O	0.59	0.44	0.31	*0.63*	*0.73*	0.46	0.47
t1.43 P_2O_5	*0.27*	*0.17*		*0.20*	*0.19*	0.16	0.12
t1.44 Total	94.8	97.3	98.0	97.8	96.8	95.0	94.4
t1.45 Mg#	49.0	47.2	53.6	53.5	51.5	48.9	49.2
t1.46 Fo source	LA	LA	LA	LA	LA	EMP	EMP
t1.47 Fo_{host}	76.6	75.4	78.6	77.3	77.3	75.7	75.7
t1.48 $Fo_{equilibrium\ olivine}$	75	71	75	79	78	76	67
t1.49 Long axis (μm)	95	125	37	75	23	250	300
t1.50 Short axis (μm)	50	55	12	60	15	155	250
t1.51 MI shape	Oval	Rectangular	Oval	Football	Oval	Oval	Oval
t1.52 MI features			b	a,b	a	a	

t1.53 Unit	ET3	ET3	ET3	ET3	ET3	ET3	ET3
t1.54 Sample name	AR0302-4a	AR0302-4a	AR0302-5a	AR0302-5a	AR0302-5b	NMNH ET3a	NMNH ET3b
t1.55 Notes	LAMI	*Replicate*	HAMI	*Replicate*	HAMI	LAMI	LAMI
t1.56 SiO_2	58.23	59.47	50.51	51.66	52.22	57.93	58.21

(continued on next page)

t1.57 Table 1 (*continued*)

	Unit	ET3	ET3	ET3	ET3	ET3	ET3	ET3
t1.59	Sample name	AR0302-4a	AR0302-4a	AR0302-5a	AR0302-5a	AR0302-5b	NMNH ET3a	NMNH ET3b
t1.60	TiO_2	1.28	1.13	0.91	0.80	0.77	1.25	1.21
t1.61	Al_2O_3	16.27	16.52	17.63	18.13	18.80	15.83	15.81
t1.62	FeO	5.81	5.48	8.00	8.01	7.14	8.50	7.36
t1.63	Fe_2O_3	1.61	1.52	2.22	2.22	1.98	2.36	2.04
t1.64	MnO	0.12	0.08	0.19	0.19	0.16	0.23	0.14
t1.65	MgO	2.68	2.55	4.21	4.15	1.99	2.24	2.10
t1.66	CaO	6.03	5.93	8.24	8.13	8.05	7.88	6.69
t1.67	Na_2O	2.44	2.59	1.74	1.99	1.98	2.99	2.85
t1.68	K_2O	0.39	0.34	0.24	0.25	0.32	0.86	0.48
t1.69	P_2O_5	*0.41*	0.36	*0.17*	0.12			
t1.70	Total	95.3	96.0	94.1	95.7	93.4	100.1	96.9
t1.71	Mg#	45.1	45.4	48.4	48.0	33.2	32.0	33.7
t1.72	H_2O (wt.%)	3.26		3.54			1.10	2.41
t1.73	CO_2 (ppm)	83.7		177.4			41.0	47.5
t1.74	F (ppm)	667		308			461	557
t1.75	S (ppm)[1]	890		2170			447	619
t1.76	S (ppm)[2]	834	970	1950	2190		567	820
t1.77	S (ppm)[3]	852		1880				
t1.78	% SO_4 of total sulfate	78%		58%				
t1.79	Log fO_2 (ΔNNO)	+0.93		+0.51				
t1.80	Cl (ppm)[1]	2570		1670			1570	1780
t1.81	Cl (ppm)[2]	2140	2540	1270	1090	1880	1970	1910
t1.82	Cl (ppm)[3]	2340		1850				
t1.83								
t1.84	*Host-corrected compositions*							
t1.85	Olivine added	2%	2%	3%	3%	12%	8%	6%
t1.86	SiO_2	57.84	59.058	50.16	51.286	50.68	56.40	57.03
t1.87	TiO_2	1.26	1.11	0.88	0.78	0.69	1.16	1.21
t1.88	Al_2O_3	15.95	16.20	17.12	17.60	16.79	14.66	14.92
t1.89	FeO	6.17	5.83	8.4	8.4	9.1	10.0	8.6
t1.90	Fe_2O_3	1.58	1.49	2.2	2.2	1.8	2.2	1.9
t1.91	MnO	0.12	0.08	0.18	0.18	0.14	0.23	0.13
t1.92	MgO	3.37	3.25	5.25	5.18	5.66	4.56	3.90
t1.93	CaO	5.91	5.93	8.00	7.89	7.19	7.30	6.31
t1.94	Na_2O	2.39	2.54	1.69	1.93	1.77	2.77	2.69
t1.95	K_2O	0.38	0.33	0.23	0.24	0.29	0.80	0.45
t1.96	P_2O_5	*0.40*	0.35	*0.17*	0.12			
t1.97	Total	95.4	96.2	94.2	95.8	94.1	100.1	97.1
t1.98	Mg#	49.4	49.9	52.7	52.4	52.5	44.7	44.8
t1.99	Fo source	EMP		LA		LA	EMP	EMP
t1.100	Fo_{host}	76.9		79.0		79.0	73.3	72.7
t1.101	$Fo_{equilibrium\ olivine}$	73	73	76	75	62	61	63
t1.102	long axis (μm)	95		205		40	35	110
t1.103	short axis (μm)	70		115		35	30	40
t1.104	MI shape	oblong	oblong	oval	oval	oval	round	hourglass
t1.105	MI features			b	b	a	a	c

	Unit	ET3	ET3	ET3	ET6	ET6	ET6	ET6	ET6	ET6
t1.107	Sample name	NMNH ET3c	NMNH ET3d	NMNH ET3e	NMNH ET6a	NMNH ET6b	NMNH ET6c	NMNH ET6d	NMNH ET6e	NMNH ET6f
t1.108	Notes	LAMI	LAMI	LAMI	LAMI	LAMI		LAMI	LAMI	LAMI
t1.109	SiO_2	55.69	58.60	58.17	53.74	51.11		56.27	54.92	53.36
t1.110	TiO_2	1.09	1.10	1.21	1.11	1.09		0.67	0.93	0.88
t1.111	Al_2O_3	15.64	16.76	15.89	17.04	16.09		18.00	17.74	17.12
t1.112	FeO	5.54	5.35	6.57	6.33	6.92		4.58	6.26	7.15
t1.113	Fe2O3	1.54	1.49	1.82	1.76	1.92		1.27	1.74	1.98
t1.114	MnO	0.19	0.16	0.14	0.15	0.17		0.14		

t1.115 Table 1 (*continued*)

t1.116 Unit	ET3	ET3	ET3	ET6	ET6	ET6	ET6	ET6	ET6
t1.117 Sample name	NMNH ET3c	NMNH ET3d	NMNH ET3e	NMNH ET6a	NMNH ET6b	NMNH ET6c	NMNH ET6d	NMNH ET6e	NMNH ET6f
t1.118 MgO	1.38	0.94	1.52	2.36	2.64		2.75	1.95	2.86
t1.119 CaO	7.07	6.44	6.97	7.80	8.11		5.62	8.79	8.56
t1.120 Na_2O	4.00	1.55	1.32	3.40	2.76		3.73	2.92	2.84
t1.121 K_2O	0.83	0.40	0.24	0.59	0.56			0.59	0.61
t1.122 P_2O_5	0.26			0.32	0.19		0.58	0.38	0.30
t1.123 Total	93.2	92.8	93.8	94.6	91.5		93.6	96.2	95.7
t1.124 Mg#	30.8	23.9	29.2	40.0	40.5		51.7	35.7	41.6
t1.125 H_2O (wt.%)	2.30			3.16	3.50	2.80	2.75		
t1.126 CO_2 (ppm)	c.c			c.c	c.c	149	137		
t1.127 F (ppm)	497			398	433	233	981		
t1.128 S (ppm)[1]	527			950	969	524	566		
t1.129 S (ppm)[2]	625	426	449						
t1.130 S (ppm)[3]				1160	1100	679	727	800	
t1.131 % SO_4 of total sulfate									
t1.132 Log fO_2 (ΔNNO)									
t1.133 Cl (ppm)1	1650			1290	1430	688	3430		
t1.134 Cl (ppm)[2]	2320	1840	1920						
t1.135 Cl (ppm)[3]				1330	1400	631	3660	2600	
t1.136									
t1.137 *Host-corrected compositions*									
t1.138 Olivine added	5%	8%	7%	3%	4%		1%	6%	3%
t1.139 SiO_2	54.80	56.95	56.78	53.27	50.61		56.18	53.94	52.91
t1.140 TiO_2	1.04	1.02	1.13	1.08	1.05		0.67	0.88	0.85
t1.141 Al_2O_3	14.90	15.52	14.85	16.54	15.47		17.91	16.74	16.62
t1.142 FeO	6.74	7.42	8.2	6.91	7.6		4.66	7.44	7.68
t1.143 Fe_2O_3	1.46	1.38	1.7	1.70	1.8		1.27	1.64	1.92
t1.144 MnO	0.18	0.15	0.13	0.15	0.16		0.14		
t1.145 MgO	2.85	3.11	3.53	3.34	3.94		2.94	3.84	3.84
t1.146 CaO	6.73	5.96	6.51	7.57	7.80		5.59	8.29	8.31
t1.147 Na_2O	3.81	1.44	1.23	3.30	2.65			2.76	2.76
t1.148 K_2O	0.79	0.37	0.22	0.57	0.54		1.53	0.56	0.59
t1.149 P_2O_5	0.24			0.31	0.18		0.58	0.36	0.29
t1.150 Total	93.5	93.3	94.3	94.8	91.9		91.5	96.4	95.8
t1.151 Mg#	43.0	42.8	43.5	46.3	47.9		52.9	31.8	47.1
t1.152 Fo source	EMP	EMP	EMP	EMP	EMP	EMP	EMP	EMP	EMP
t1.153 Fo_{host}	72.0	72.0	72.0	74.7	74.9	76.4	79.0	74.9	74.9
t1.154 $Fo_{equilibrium\ olivine}$	60	51	58	69	69		78	65	70
t1.155 Long axis (μm)	35	25		60	40	30	40		
t1.156 Short axis (μm)	30	20		40	35	22	25		
t1.157 MI shape	Round	Oval	Round	Rectangular	Round	Round	Oval		
t1.158 MI features				a	c				

Major elements in melt inclusions were acquired by EMP at either the AMNH or MIT (in italics) except for NMNH ET6e and ET6f, which are reproduced from Melson (1983). H_2O, CO_2, and F data collected by SIMS at DTM, 'c.c' indicates carbon contamination. S and Cl data were collected at 3 different labs, indicated by footnotes: 1=SIMS at DTM; 2=EMP at MIT; 3=EMP at AMNH. See Section 3.1 of the text for a discussion of accuracy and inter-lab calibration. Percent sulfate determined by S–Kα shift analyses at AMNH. log fO_2 calculated at 1100 °C and 3 kbar from Huebner and Sato (1970). FeO−Fe_2O_3 calculated assuming 20% total Fe as Fe^{3+} (based on fO_2 from S–Kα and pMELTS Fe-speciation model (Ghiorso et al., 2002)). Melt inclusion major element compositions have been corrected for sidewall crystallization by adding equilibrium olivine back into the glass composition in 1% increments until the glass was in equilibrium with the adjacent host. Fo (molar Mg/(Mg+Fe)) acquired by either EMP at MIT or LA-ICP-MS at BU. MI features: a=vapor or shrinkage bubble present,b=oxide crystal present, c=fracture
t1.159 running through.

AR0301 and AR0302 samples were collected for this study from tephra units ET3 and ET6 (originally defined by Melson (1983) and recently renamed AR-19 and AR-16, respectively, by Soto and Alvarado (this issue)). NMNH samples are thin sections from the Smithsonian National
t1.160 Museum of Natural History (ET3 ID: 113852-3.4; ET6 ID: 113852-3.2).

remainder was gently crushed in an alumina jaw-crusher and sieved for mineral picking.

3.1. Melt inclusions: major, trace, and volatile element analyses

While picking olivine-hosted inclusions, we sought naturally glassy melt inclusions, avoiding those that were cracked or breached, or touching the outer edge of the host olivine. Olivines were very rare in the fractions picked (ranging from 250–1000 μm), averaging only one olivine grain per 150 g of sample. Of those olivines, ~ 30% yielded viable inclusions. Olivines were polished to expose inclusions, and then mounted either directly in indium metal (to minimize background in the ion probe; Hauri et al., 2002), or first in dental resin to be transferred to indium for volatile analysis.

Major element, S, and Cl concentrations in some inclusions were determined by electron microprobe on a JEOL JXA-733 Superprobe at the Massachusetts Institute of Technology using a 10 nA beam current, 10 μm spot, and 15 kV accelerating voltage. Elements were counted for 40 s, except for Na which was counted for 5–10 s. Major element concentrations were also determined on a Cameca SX 100 electron microprobe at the American Museum of Natural History using somewhat different conditions: 10 nA, 12 μm, and 15 kV, with on-peak count times of 30 s. Chlorine and sulfur were acquired at 40 nA, 12 μm, and 15 kV. Low totals in some samples are most likely due to alkali loss (especially Na) during analysis, a common consequence of electron probe analysis of hydrous glass (Devine et al., 1995). Uncertainty on S and Cl by EMP is ~ 3% at AMNH (based of replicate analyses of the JDF glass standard in one session) and <12% at MIT (based on replicate analyses of inclusions in 2 separate sessions).

Volatile (H_2O, CO_2, F, Cl, and S) concentrations in melt inclusions were determined at the Carnegie Institution of Washington using a Cameca 6-F ion microprobe using an 8 nA beam current, 30 μm spot, 5 kV accelerating voltage. On-peak count time was ~ 5 s, and other protocols followed those in Hauri (2002). Some inclusions which had been carbon-coated for EMP analysis prior to SIMS yielded very high CO_2 concentrations (1000's of ppm CO_2) which we interpreted as carbon contamination (Table 1). Precision on the SIMS (at DTM) is <1.5% 2σ based on replicate analyses of melt inclusions during the same session. However, the accuracy may be closer to 10% based on uncertainty in the working curves developed for each session. Because S and Cl contents were determined in 3 separate labs, during 7 different sessions, there is variability between multiple analyses of single inclusions. Lab-to-lab variations arise from the different standards and calibration strategies used, for example the use of sulfide standards versus natural glasses (typically MORB), none of which are ideal for arc melt inclusions. Nonetheless, replicate analyses agree on average by 12% (for S) and 9% (for Cl).

Wavelength dispersive S Kα scans were performed on 5 inclusions to determine speciation of dissolved S (Wallace and Carmichael, 1992). Analyses were performed by EMP at the AMNH, following the methods of Mandeville et al. (in review). FeS and $BaSO_4$ were analyzed as in Carroll and Rutherford (1988), using a 40 nA beam current, 12 μm spot, and 15 keV accelerating voltage. Twelve to sixteen continuous S X-ray scans were carried out for each inclusion, and the beam was moved within the inclusion every 4–5 accumulations, in order to avoid oxidation effects due to local heating (Wallace and Carmichael, 1992; Metrich and Clocchiatti, 1996). fO_2 was calculated from the sulfur-speciation model of Wallace and Carmichael (1994).

Trace element concentrations were determined in inclusions larger than 50 μm in diameter by laser ablation inductively coupled plasma mass spectrometry (LA-ICP-MS) at Boston University using a Merchantek/VG Microprobe II 213 nm Nd-YAG laser ablation system coupled to a VG PQ ExCell quadrupole ICP-MS. Samples were ablated in a He–Ar mixture at a flow rate of 700 mL/min. The laser was operated in spot-drill mode at 5 Hz, at 80% power (0.118–0.137 mJ/pulse), for an energy density of ~ 6 J cm^{-2}. The beam expander (collimator) and iris were both set to 0%, resulting in a spot size of 40 μm. Dwell time for all elements was 20 ms. Laser data were acquired in time-resolved mode, and calibrated against USGS glass BHVO-2 g using the values in Kelley et al. (2003), with ^{43}Ca as an internal standard. Precision on replicate analyses of BCR-2 g was 8% rsd.

3.2. Bulk-rock major and trace element analyses

In order to provide context for the melt inclusions from newly-sampled material, host bulk−rocks were analyzed for major and trace elements at Boston University, following the techniques described by Kelley et al. (2003). Solutions were prepared for major element analysis using $LiBO_2$ fusions, and each resulting solution was diluted ~ 4300× the original sample weight. Ten major elements were measured in these solutions using a Jobin–Yvon 170C ICP-AES. Sample powders were prepared for trace element analysis following HF–HNO_3 digestion in Teflon screw-top vials, and resulting solutions were diluted to ~ 2000× the original powder weight. Thirty trace elements were measured in these solutions using the VG PQ

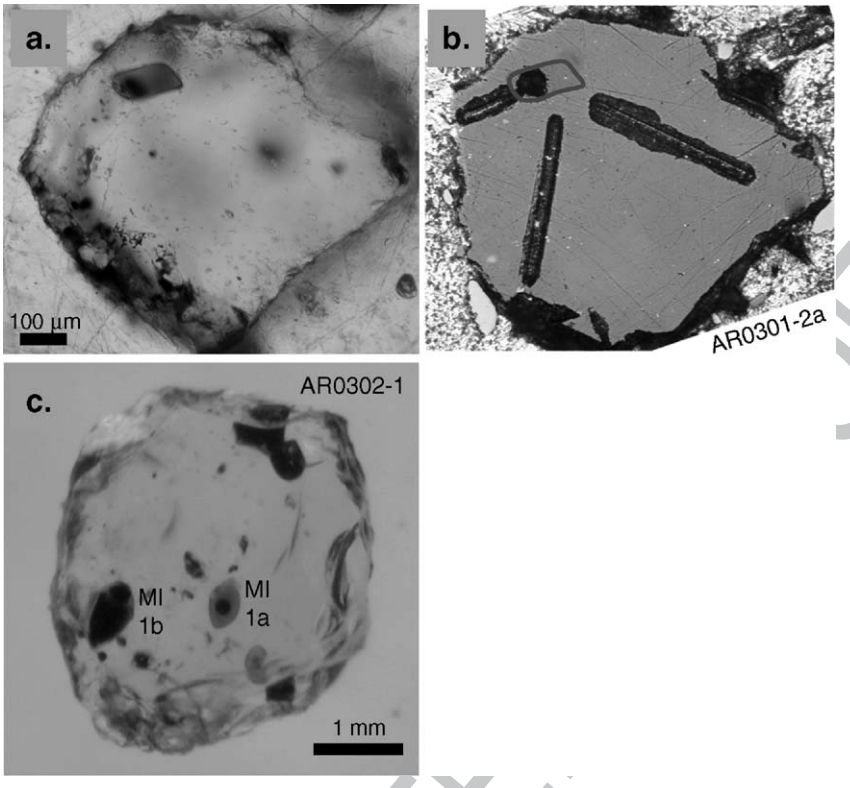

Fig. 3. Photographs of Arenal ET3 olivine-hosted melt inclusions. a) Transmitted-light photograph taken pre-ablation. b) Reflected-light photograph taken post-ablation, showing LA-ICP-MS raster tracks used to measure olivine Fo and ablation pit used to measure trace elements in glass. c) AR0302-1a and 1b are the ET3 inclusions with the highest-measured water contents (both ~ 3.9 wt.% H_2O).

ExCell quadrupole ICP-MS at Boston University. Raw ICP-MS and ICP-ES counts were blank-subtracted, corrected for drift using an external solution (analyzed every 5 samples), and corrected for the dilution weight. USGS standards BHVO-1 and BIR, as well as internal lab standards K1919 and MAS1722 were used as calibration standards, using the values in Kelley et al. (2003). Reproducibility of replicate ICP-ES and ICP-MS analyses is generally <3% rsd.

3.3. Olivine hosts: major and trace element analyses

Major element concentrations in olivines were determined by electron microprobe on a JEOL JXA-733 Superprobe at MIT, using the same conditions as the glass, although on-peak counting times were 60 s for Fe, 20 s for Na, Ca, and Si, and 40 s for all other elements, and at the AMNH, with on-peak counting times of 20 s for Na and Al, and 30 s for all other elements (Fig. 3). Transition metal, and Mg, and Fe concentrations were measured at BU by LA-ICP-MS as above, except the laser was operated in line scan (raster) mode at 10 Hz, 50% power (0.176 mJ/pulse), and a scan rate of 3 µm/s. Raster width was ~ 20 µm, with the beam expander (collimator) set to100%, and the iris to 10%. Dwell time for all elements was 20 ms. Laser data were acquired in time-resolved mode, and calibrated against USGS standard BIR-1g. Reproducibility of forsterite in the San Carlos Olivine standard was <1% 2σ (Table A1).

4. Results

4.1. Whole-rock compositions

Tephra from ET3 and ET6 contain some of the highest MgO, FeO, CaO, and Al_2O_3, and lowest Na_2O reported for Arenal (Fig. 4; Table 3). The new ET3 samples reported here (AR0301 and AR0302) are basalts (50–52 wt.% SiO_2; Mg#=53) and fall within the range of previous ET3 analyses, correlating with the high Al_2O_3 (>20 wt.%), CaO (~ 11 wt.%) and Ba/La (>43) of the base of the ET3 section (Bolge et al., 2004; Fig. 5). Some of these chemical characteristics are thought to derive from excess plagioclase at the top of the magma body prior to eruption of ET3 (Bolge et al., 2004).

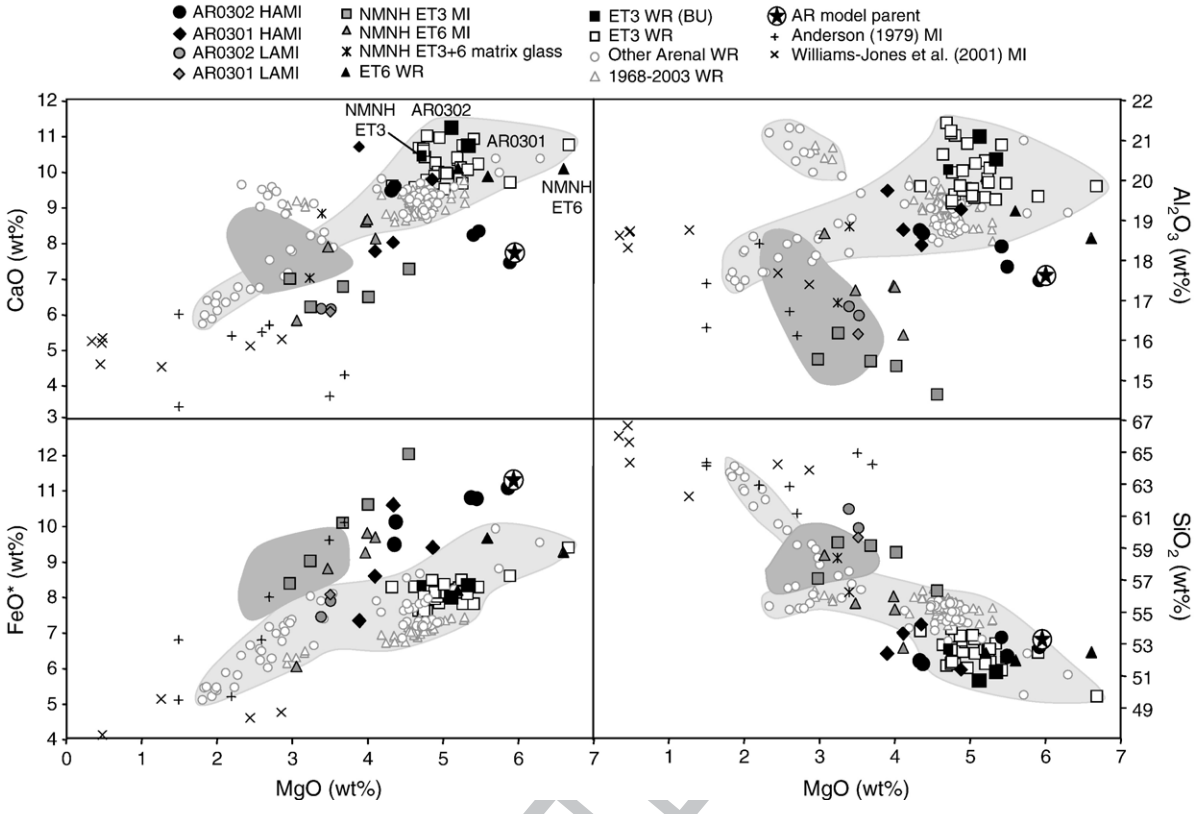

Fig. 4. Major element variations in Arenal whole rocks, as well as melt inclusions from ET tephras. Whole rocks studied here labeled in panel a. Olivine-hosted MI, as well as matrix glass from ET3 and ET6 are from this study and Melson (1983; Table 1). Large, light gray field encompasses Arenal whole rocks (Carr et al., 2003; data points shown); small, darker gray field encompasses the main population of ET3 matrix glass from Bolge et al. (2004); data points not shown. Pyroxene, plagioclase, and magnetite-hosted melt inclusions from the current eruption from Anderson (1979), and pyroxene-hosted inclusions from Williams-Jones et al. (2001). Point labeled "1968–2003 WR" from Ryder et al. (this issue). Melt inclusion compositions from this study have been corrected for post-entrapment olivine crystallization (Table 1). All compositions plotted have been normalized to volatile-free, 100% totals, except those melt inclusions in Table 1 that have low totals (<96%, in part due to alkali loss). In these cases, compositions have been normalized volatile-free, assuming an original total of 96%, in order to prevent over-correction.

4.2. Olivine phenocrysts

Nineteen olivines from ET3 and five from ET6 were analyzed for major and, in some cases, trace element concentrations (Table A1). Fig. 6 shows a histogram of the olivine population from ET3 samples AR0301 and AR0302. Cores range from Fo_{76} to Fo_{81} and rims range from Fo_{75-68}, and thus the olivine grains as a group show normal zoning. The upper range of the olivine forsterite contents (Fo_{81}) is the dominant population, and is in approximate equilibrium with the whole rock Mg# (assuming $K_{D\,(Oliv-Liq)}^{Fe/Mg}=0.3$ and $Fe^{3+}/Fe^{\Sigma Fe}=10–20\%$). The olivine rims approach composition in equilibrium with ET3 matrix glass (from Melson, 1983; Fig. 7). Thus the olivines in these ET3 samples could have formed by closed-system crystallization, with the first olivines crystallizing from the bulk magma, and later olivines and rims forming from the residual liquids. In comparison, the current eruption includes rare olivines (Streck et al., 2005), and while some compositionally overlap with those from ET3 (Fig. 6), the population's peak is shifted to lower mean Fo contents (< Fo_{75}), consistent with the more evolved whole rocks observed.

4.3. Melt inclusions—major elements and trace elements

Fifteen olivine-hosted melt inclusions from ET3 and four from ET6 were analyzed for this study. All but one inclusion (NMNH ET3b) are fully enclosed, with round, oval, oblong, or rectangular morphologies (Table 1). Fig. 7 shows the Mg# of the melt inclusions plotted against the Fo content of the host olivines. As is commonly observed, Arenal melt inclusions have Mg#'s that are too low to be in equilibrium with their host olivines. This is typically interpreted as a result of post-entrapment crystallization of olivine within the melt inclusion during cooling (e.g.,

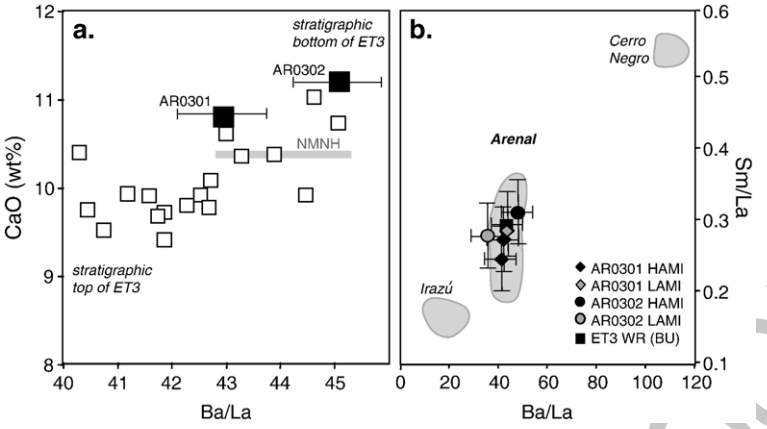

Fig. 5. a) The two ET3 samples studied here derive from the base of the ET3 tephra unit, where both CaO and Ba/La are highest (white squares are ET3 whole rocks from Bolge et al., 2004). Line marks the expected position of the NMNH ET3 sample within Bolge et al.'s geochemical stratigraphy, given its CaO content (Table 3). Error bars represent 3% uncertainty based on replicate analyses. b) Trace elements systematically vary along the Central American arc, and the Arenal MI fall within the range of Arenal whole rocks (shaded field). Irazú and Cerro Negro, and Arenal whole rock data from Carr et al. (2003). Error bars represent 8% uncertainty (Table 4).

Cervantes and Wallace, 2003). Notably, however, a few ET3 melt inclusions are in actual equilibrium with their olivine hosts (Fig. 7), and so were likely trapped at a temperature similar to that of the pre-eruptive magma. Melt inclusions trapped in higher-Fo olivines (> Fo_{75}) tend to be closer to equilibrium with their hosts than those trapped in lower-Fo olivine (< Fo_{75}). The six inclusions hosted in the lowest-Fo olivines are from the NMNH ET3 and ET6 thin sections, and all have low Al_2O_3 (see below). We assume that post-entrapment crystallization is the main process that has led to a lack of equilibrium between melt inclusion and host, and to correct for this, we added equilibrium olivine in 1% increments into glass compositions until glass and olivine host satisfied K_D (as above). The amount of olivine that was added to achieve equilibrium ranged from 0–12%, and averaged 4% (Table 1), typical again of other studies (Sisson and Layne, 1993; Cervantes and Wallace, 2003).

Melt inclusion compositions range from basalt to andesite (~ 50–59 wt.% SiO_2), whether considering the uncorrected data and or the data corrected for post-entrapment crystallization of olivine (Table 1). Once renormalized to volatile-free compositions, the melt inclusions shift to a higher range in SiO2 (~ 51–61 wt.%)and fall generally within the range of other Arenal whole rocks in MgO and SiO_2 (Fig. 4). Notably, FeO in the renormalized melt inclusion compositions are higher than the whole rock compositions, and so have not suffered from the kinds of

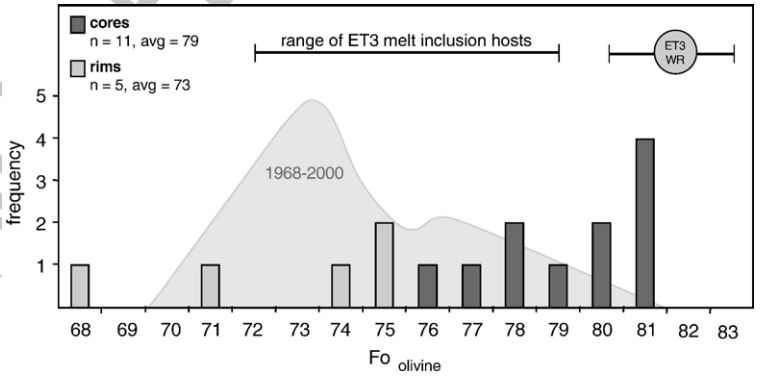

Fig. 6. Histogram of the olivine analyses from ET3 samples AR0302 and AR0301. Some olivines were analyzed in multiple locations within the same grain (see Table A1). Forsterite content (Fo) in equilibrium with whole rocks is plotted as a circle, assuming $K_D^{Fe/Mg}$=0.3 and 5–20% of total Fe in the melt is Fe^{3+}. Also shown is the total range of Fo contents of olivines that host melt inclusions. The shaded field encloses a compilation of microprobe analyses of olivine from the current eruption for comparison after Fig. 2c in Streck et al. (2005). Their olivine frequency was reduced by a factor of 6 to fit the figure.

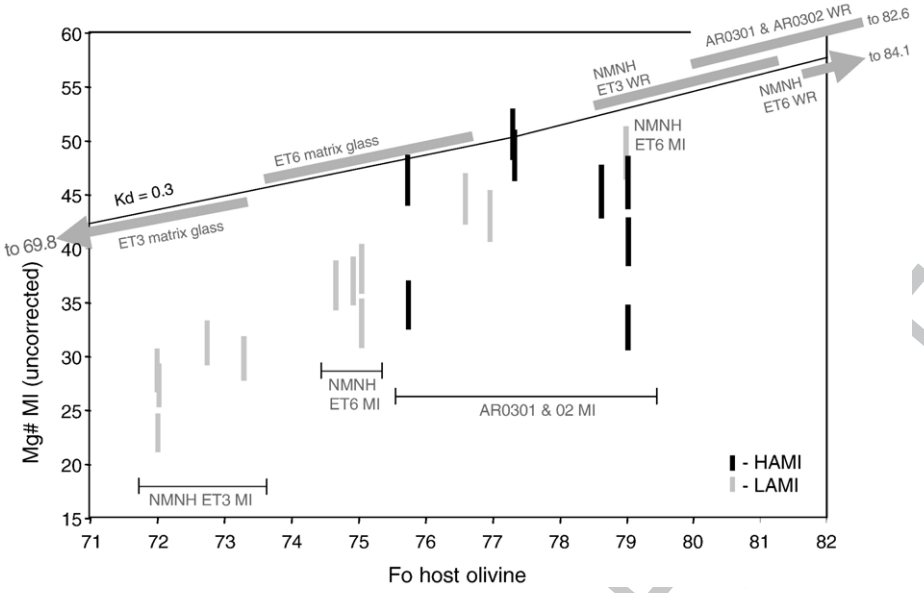

Fig. 7. Mg# of the melt inclusion versus forsterite of the adjacent olivine. These melt compositions have not been corrected for post-entrapment crystallization (e.g. raw EMP data, Table 1). The curve plotted $K_D^{Fe/Mg}=0.3$) represents equilibrium between inclusion and host. Data (from Table 1) are plotted as bars, for which $Fe^{3+/\Sigma Fe}$ in the melt is allowed to vary from 5% (bar bottom) to 20% (bar top). Also shown are compositions along the curve that would be in equilibrium with various relevant whole rock and glass compositions.

Fe-loss effects described by Danyushevsky et al. (2004; Fig. 4). However, nearly all inclusions have lower Al_2O_3 than Arenal whole rocks at the same MgO (including all ET3 and ET6 whole rocks; Fig. 4). Not only are they low, but they break into two groups of high- and low-Al, which correlate with volatile concentrations (discussed below). For this reason, we will hereafter refer to the two groups as HAMI (High Aluminum Melt Inclusions, with > 16.5 wt.% Al_2O_3 in the olivine-corrected compositions in Table 1) and LAMI (≤ 16.5 wt.% Al_2O_3). Note that these groups are different from those defined by Borgia et al. (1988), which were based on whole rock compositions and discriminated by a much higher Al_2O_3 (20 wt.%). AR0301 HAMI have slightly higher Al_2O_3 than the HAMI from AR0302. The LAMI form a systematic trend in their disequilibrium from host olivines (Fig. 7), and in general represent more modified compositions. In fact, there are no volcanic rocks erupted from Arenal that overlap with the LAMI, although many overlap with ET3 matrix glass compositions (Bolge et al., 2004; Fig. 4).

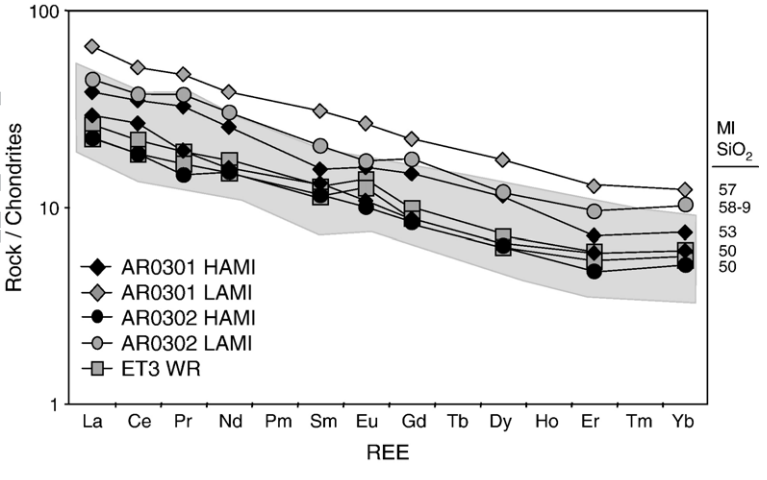

Fig. 8. Chondrite-normalized rare earth element (REE) patterns for Arenal MI's and whole rocks (Table 4). The shaded field encloses Arenal whole rock data (sources as in Fig. 2).

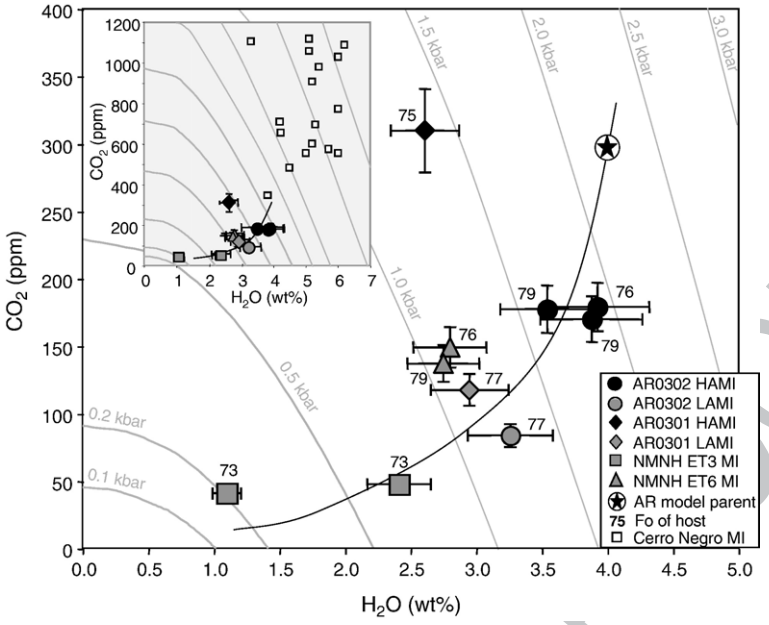

Fig. 9. Volatile (H_2O and CO_2) concentrations in Arenal melt inclusions, plotted with vapor saturation isobars calculated for basaltic melts from VolatileCalc (Newman and Lowenstern, 2002). Samples compromised by carbon contamination not plotted, but listed in Table 1. Error bars indicate 10% rsd, external SIMS precision (see Section 3.1 of text). Solid black curve traces a closed-system degassing path assuming starting conditions of 1100 °C, 10% exsolved vapor, and 49% SiO_2. Fo of host olivine decreases with progressive degassing. Inset relates Arenal MI to Cerro Negro MI Cerro Negro data from Roggensack et al., 1997, 2001a.

Melt inclusion REE patterns are nearly parallel to each other, as well as to most whole-rocks from Arenal (Fig. 8). REE concentrations rise with SiO_2 and P_2O_5, and decreasing MgO, consistent with magma fractionation. Trace element ratios (e.g. Sm/La and Ba/La; Fig. 5b) fall within the range for other Arenal rocks. Ba/La in the AR0301 melt inclusions (41–43) is nearly identical to that in the AR0301 whole rock (43; Fig. 5b). The AR0302 melt inclusions include an anomalously low Ba/La value (35) and one (48) that is similar to the whole rock value (45). The similarity in Ba/La between the ET3 melt inclusions and whole rocks provides evidence that the melt inclusions are indeed derived from ET3 magma, and that ET3 whole rock Ba/La is not strongly affected by plagioclase accumulation.

4.4. Melt inclusions—volatile content

Water concentrations in Arenal melt inclusions range from 1.1 to 3.9 wt.% (Table 1, Fig. 9). These values correlate broadly with host Fo content (Fig. 9) and the SiO_2 concentration in the melt inclusion (Fig. 2a), reflecting coupled crystal fractionation and H_2O degassing. CO_2 in the melt inclusions varies from 50–300 ppm, and describes what is best modeled as a closed-system degassing trend with H_2O (Fig. 9). Mixed H_2O–CO_2 vapor-saturation isobars suggest that the highest-H_2O inclusions from Arenal were trapped at ~ 2 kbar, and the lowest at ~ 0.2 kbar (Fig. 9). HAMI were trapped at higher pressures (>1.2 kbar) than LAMI, as indicated by their higher H_2O and CO_2 contents. These pressures are minima, however, as S and Cl will lower CO_2 and H_2O solubility in melts, and so raise vapor saturation pressures (Webster, 2005). Based on crystal–melt equilibria, Reagan et al. (1987), Cigolini (1998) and Ryder et al. (this issue) estimate 4–10 kbar crystallization pressures for modern Arenal magmas.

The melt inclusions with the highest water concentrations also have the highest sulfur (~ 3000 ppm; Fig. 10a), and H_2O and S together define a degassing trend analogous to that of H_2O and CO_2. Modeling such a trend is more difficult than for H_2O–CO_2, given the lack of experimental constraints on sulfur solubility in melts that are saturated with a mixed vapor, and the complication of multiple sulfur species as a function of oxidation state (Wallace and Carmichael, 1992). We thus take the approach of Sisson and Layne (1993), and calculate a degassing path based on a constant partition coefficient between vapor and melt, and independent constraints on the modal proportion of vapor, liquid, and crystals, derived from the H_2O–K_2O relationships (Fig. 10a). While this exercise does not take into account the importance of T, P,

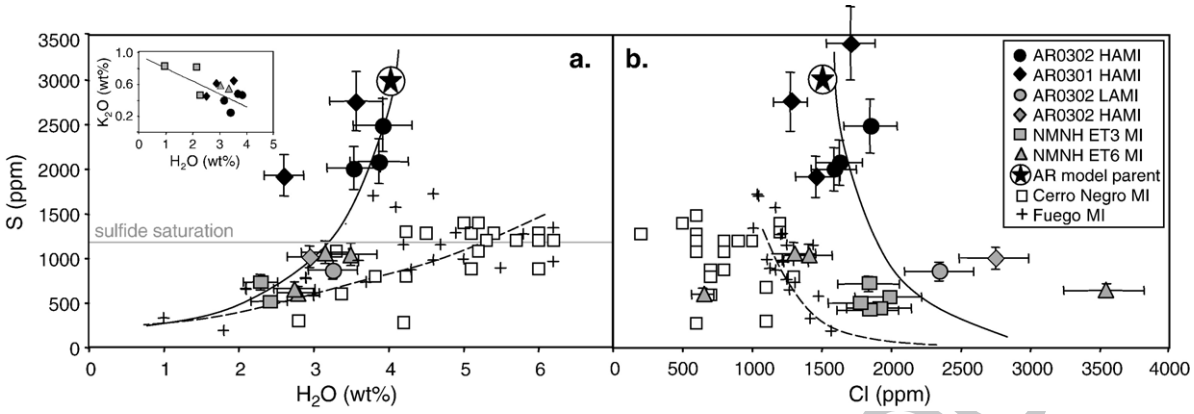

Fig. 10. Water, sulfur, and Cl degassing in Arenal MI's, compared to other Central American MI's. The solid degassing paths are after Fig. 6 in Sisson and Layne (1993), calculated for Arenal assuming a constant $D_S^{fluid/melt}=70$ and $D_{Cl}^{fluid/melt}=6$. The dashed lines are Fuego S and Cl degassing paths from Sisson and Layne (1993). Inset shows K_2O–H_2O data used to calculate the proportion of H_2O vapor in the bulk separating assemblage (line shows model for 6% H_2O vapor, assuming $K_{D(Xtal-Melt)}=0$ for K_2O. Sulfide solubility from Wallace (2005), and corresponds to the limit for sulfide-saturated basaltic melt (1150 °C, 8 wt.% FeO^T, 1 bar and NNO-2). Cerro Negro data from Roggensack et al. (1997) and Roggensack (2001a), Fuego data from Roggensack (2001b) and Sisson and Layne (1993). Error bars for H_2O indicate 10% rsd. S and Cl plotted as average (+/− SD) of the multiple measurements listed in Table 1. If single measurements were made, error bars are the average uncertainty (12% for S and Cl; see Section 3.1 of text).

and fO_2 controls on sulfur solubility, it does at least provide a comparison to Sisson and Layne's calculation for Fuego melt inclusions. We can create the Arenal S–H_2O degassing path given 6 wt.% vapor in the bulk separating assemblage (e.g. with the other 94% being crystals), and a $D_{(vapor/liquid)}$ for sulfur of 70. This calculation is consistent with the H_2O–CO_2 path shown in Fig. 9, as the vapor is dominated by H_2O along the path (>97 wt.%; Newman and Lowenstern, 2002). The parameters calculated above for Arenal are broadly similar to those estimated for Fuego, with Arenal having slightly less H_2O in the mode (6% vs. 8% for Fuego) and a higher D for S (70 vs. 34 for Fuego). The differences are consistent with Arenal melts having lower overall water contents (1–4 wt.% vs. 1–6 wt.% for Fuego), and so less water vapor in the mode. Arenal melts also record lower vapor saturation pressures (<2 kbar vs. >3 kbar for Fuego), consistent with a lower sulfur solubility in the melt (higher D).

The calculated sulfur degassing curve passes through all of the ET3 and ET6 melt inclusions, except for two HAMI from AR0301. Melts from this sample appear to have lower water for a given sulfur, which could be a primary feature of the parental melt. All of the LAMI have <1200 ppm S, and so reflect more degassed compositions than HAMI. K-α measurements indicate that most of the sulfur dissolved in Arenal melt inclusions is speciated as sulfate (58–84% of total sulfur; Table 1), which means that none of the MI contain enough sulfide species to saturate a sulfide phase (assuming 1200 ppm as the limit of sulfide solubility in melts with ≤8 wt.% FeO^T; Wallace and Carmichael, 1992; Fig. 10a). The high sulfur concentrations in least degassed Arenal melt inclusions, many >2000 ppm, also appear to reflect a lack of sulfide saturation during mantle melting, and possible excess sulfur in the mantle source (Wallace, 2005). The measured sulfur species, combined with the formulations in Wallace and Carmichael (1992) yield a range of fO_2 from 0.5 to 1.1 log units above NNO, or an average fO_2 of NNO+0.9 (Table 1). Such high fO_2 estimates are typical of arc magmas (Carmichael, 1991; Wallace and Carmichael, 1992, 1994; Metrich and Clocchiatti, 1996; Wallace, 2005) and fall within the range of estimates made for Arenal by some previous workers. Reagan et al. (1987) calculate ~ NNO+0.3 based on coexisting titanomagnetite and ilmenite grains in a gabbroic xenolith expelled during the recent eruption, while Beard and Borgia (1989) calculate NNO+1 based on magnetite in gabbroic enclaves. Ryder et al. (this issue) conclude that fO_2 must be at least QFM+2 (~ NNO+1.2) in order to match the fractionation assemblage of Stage 1 (1968–1971) Arenal magmas. With the exception of the higher gabbroic estimates in Cigolini (1988) (~ NNO+2), most studies, including the melt inclusion-derived estimates here, thus support fO_2 in the range from NNO+0.5 to+1 for Arenal mafic magmas.

In contrast to the progressive degassing of H_2O, CO_2, and S (Figs. 9, 10), Arenal melt inclusions record increasing concentrations of F and Cl with SiO_2 (Fig. 11). This is consistent with the higher solubility of F and Cl (relative to H_2O, CO_2 and S) in mafic to intermediate melt compositions (Webster, 2004). Similar degassing calculations

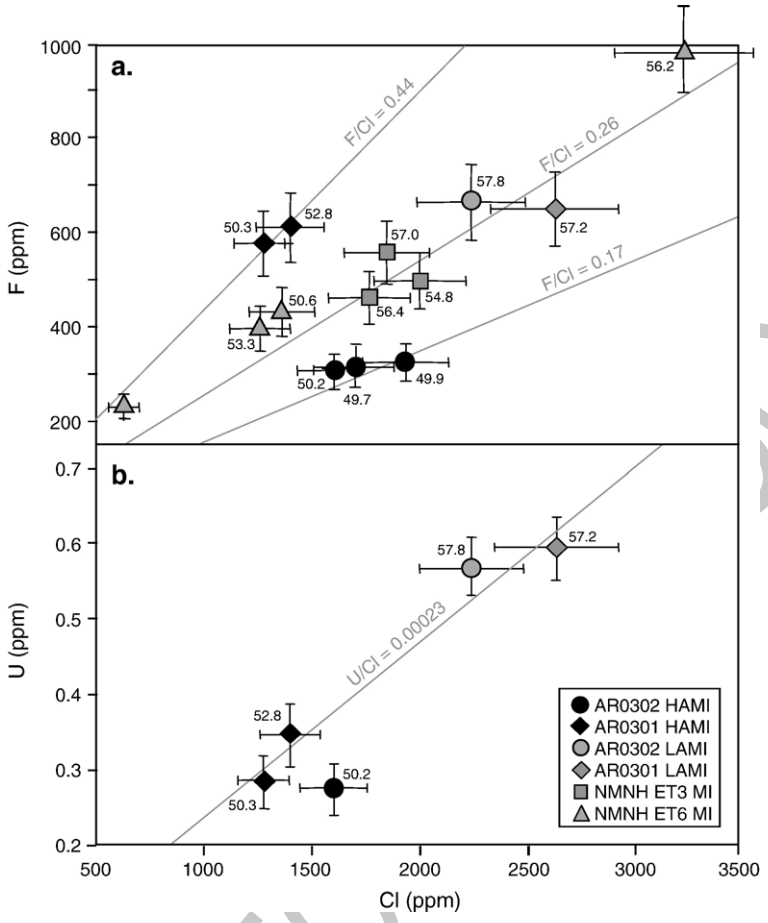

Fig. 11. a) Cl vs F and b) Cl vs. U in Arenal melt inclusions (Tables 1, 3). As Cl and F increase during fractionation, so do incompatible elements such as U. Values adjacent to data points denote olivine-corrected SiO_2 content of the inclusion in wt.%. The ET6 point without a SiO_2 value was not analyzed for major elements (Table 1). Lines of constant ratio are shown for reference. Error bars indicate 8% rsd for U, and 9% for F and Cl (see Section 3.1 of text).

for S and Cl predict a $D_{(vapor/liquid)}$ of 6 for Cl, although value between 0 and 13 will produce a degassing curve that passes through some portion of the melt inclusion data. The lower D values, however, are consistent with the greater melt solubility of Cl than S, and the incompatible behavior of Cl. Chlorine correlates well with other trace elements, such as U (Fig. 11b), that are highly incompatible in crystals and vapors under these conditions. Cl and F also correlate well in the ET6 melt inclusions, and within HAMI from different samples (Fig. 11a). Different F/Cl variations may reflect different parental magma compositions for ET6, and different phases of the ET3 eruption. ET6 melt inclusions also appear to have lower Cl for the same S as ET3 inclusions.

In summary, the most primitive melt inclusions from Arenal are high-alumina basaltic liquids hosted in $Fo_{76–79}$ olivines and contain up to 4 wt.% H_2O, >200 ppm CO_2, >2000 ppm S, ~ 1500 ppm Cl and >300 ppm F. The olivines that host these melt inclusions are near equilibrium with whole rock compositions, and the melt inclusions have trace element ratios similar to those in the whole rock hosts. Thus these volatile estimates are reasonable for the ET3 parent magma. The ET6 melt inclusions are more evolved, but have similar H_2O–CO_2 and S histories to the ET3 magmas, and so presumably reflect a magma with a similar volatile budget to ET3 (albeit with slightly different Cl and F). Taken as a whole, the melt inclusions record the systematic degassing of H_2O, CO_2, and S upon ascent from >2 kbar to 0.2 kbar. Measures of magma differentiation, such as Si, K and Fo covary with volatile contents, suggesting a coupled process of ascent, degassing, and crystallization. The most degassed melt inclusions, with H_2O–CO_2 vapor saturation pressures of <1.2 kbar, also have unusual, low-Al compositions that are unlike most volcanic rocks from Arenal.

5. Discussion

5.1. Implications for the differentiation of Arenal magmas

The data we report here for Arenal melt inclusions provides us with the opportunity to reassess petrologic models for the differentiation of Arenal magmas. Most rock samples collected from arc volcanoes are mixtures of crystals and liquid to varying degrees. This is especially true of Arenal, where a high degree of crystallinity, in the form of phenocrysts (Bolge et al., 2004), xenocrysts (Streck et al., 2004) and xenoliths (Reagan et al., 1987; Beard and Borgia, 1989; Cigolini, 1998), is widespread in mafic and intermediate eruptives. Melt inclusions represent rare samples of magmatic liquid, and can clarify the relative role of liquid and crystal in making up whole rock compositions, and the extent to which whole rocks represent liquid compositions.

Here we provide an overview of the compositional spectrum of Arenal volcanic rocks. Our inferences are based largely on MgO–Al_2O_3 systematics, as alumina has long been recognized as a dominant vector of variability in Arenal volcanics, and relates directly to processes involving plagioclase, the dominant crystalline phase (Borgia et al., 1988; Bolge et al., 2004) and (Fig. 12). We begin with the premise that the HAMI of ET3 are potential liquids. These inclusions represent melt trapped at the highest pressures, have the least degassed compositions, and are closest to equilibrium with the host olivines. It follows that their major element compositions are the closest to actual parental Arenal liquids.

In order to facilitate discussion of magma variation, we present a model composition which we believe to be the best estimate of an Arenal parent magma (Table 2). We start with the major element composition of the highest MgO melt inclusion (after olivine-correction, AR0302-5b). Because Na_2O in this MI was likely lost during the microprobe analysis, and P_2O_5 was not measured, we use values appropriate to whole rocks in the same compositional range. A water content of 4.0 wt.% was chosen to reflect the maximum measured in Arenal melt inclusions (3.93 wt.%), Other volatile species were chosen to be consistent with H_2O of 4 wt.%, given the trends in Figs. 9 and 10 and F/Cl of 0.2 (Fig. 11). The composition was then re-normalized to 100% (both including the volatiles, and without; Table 2). Clearly more than one parental magma feeds the Arenal system, but the compositional features of this parent provides a useful reference to the whole rock population.

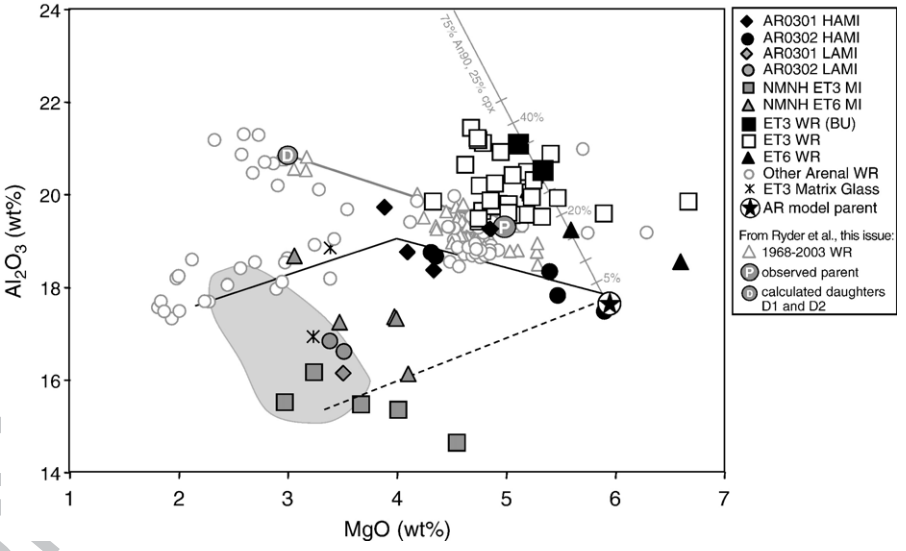

Fig. 12. Al_2O_3 variation with MgO in Arenal whole rocks and melt inclusions. Data sources and corrections/normalizations as in Fig. 4. Small gray field encompasses main population of ET3 matrix glass (Bolge et al., 2004). Thin gray line calculated by mixing between model parent (Table 2) and end-member cumulate assemblages containing plagioclase and cpx in the proportion indicated. Tick marks on the line represent 5% total crystal addition. Lower, dashed black line is liquid line of descent (LLD) generated from MELTS (Ghiorso and Sack, 1995) with 0.5 wt.% H_2O at 500 bars. Black solid line is LLD generated from pMELTS (Ghiorso et al., 2002) with 3.5 wt.% H_2O at 3 kbar. We chose to use pMELTS for the high H_2O and high pressure LLD because it includes significantly more phase equilibrium constraints at >1 atm pressure, as well as an improved reference model for the state properties of water dissolved in melt (Ghiorso et al., 2002). MELTS is preferred for low-P, low-H_2O calculations (Asimow et al., 2004). The clinopyroxene used for mixing calculations contains 5 wt.% Al_2O_3 and 15 wt.% MgO. Thick gray line represents the possible LLD from the observed parent of Ryder et al. (this issue) to their calculated daughter compositions.

Table 2
Composition of the Arenal model parent

SiO_2	51.00
TiO_2	0.73
Al_2O_3	16.89
FeO	9.30
Fe_2O_3	1.88
MnO	0.18
MgO	5.70
CaO	7.43
Na_2O	2.42
K_2O	0.29
P_2O_5	*0.19*
Total	96.0
Mg#	52.2
H_2O (wt.%)	4.00
CO_2 (ppm)	300
F (ppm)	300
S (ppm)	3000
Cl (ppm)	1500

Based on one of the most primitive ET3 HAMI (AR0302-5b) and calculated as discussed in Section 5.1 of the text.

In comparison to the HAMI and the model parent, virtually all the ET3 whole rock samples are enriched in Al_2O_3, some by several wt.% Al_2O_3 (up to 21 wt.%; Fig. 12). If the HAMI are liquids, then these whole rock samples are derived from more aluminous parents, or have accumulated aluminous crystals. The fact that ET3 whole rocks are otherwise similar to their melt inclusions (e.g. in terms of Ba/La and REE, Figs. 5 and 8), does not support a wide variation in parental compositions. Instead, it is more likely that the ET3 whole rocks are not liquids, but have accumulated an aluminous crystal assemblage. This is supported by petrographic observations, modal analyses, and least squares mixing calculations of ET3 whole rocks samples (Borgia et al., 1988; Bolge et al., 2004). Moreover, the REE patterns of our ET3 samples (the whole rock hosts to the melt inclusions) possess large positive Eu anomalies (Eu/Eu* of ~ 1.25, where Eu* is the Eu chondrite-normalized concentration interpolated between Sm and Gd; Fig. 8; Table 4), which is a common feature of the ET3 whole rock population (Bolge et al., 2004). Such an Eu anomaly can be generated by up to 30% accumulation of plagioclase (assuming Sm = 0.17, Eu = 0.37 and Gd = 0.13 ppm; as in some Arenal plagioclases, Reagan et al., this issue). In agreement with this result, crystal accumulation calculations (Fig. 12) also show that the ET3 whole rock hosts (with >20 wt.% Al_2O_3) can be produced from the model parent by 30–40% accumulation of mixtures of plagiolcase (An_{90}) and cpx, phases which are commonly observed as crystal clots (Borgia et al., 1988) cognates (Beard and Borgia, 1989) or glomerocrysts (Borgia et al., 1988). Thus, it seems reasonable that virtually all of the ET3 whole rocks have accumulated excess plagioclase and clinopyroxene, and that the melt inclusions provide better samples of true liquid compositions.

Although from a different eruption, our ET3 melt inclusions may also contribute to the understanding of the current, on-going eruption. While most of our HAMI have lower Al_2O_3 than any modern Arenal whole rocks, two HAMI from AR0301 overlap the whole rock compositions from the on-going eruption (Fig. 12). One of the inclusions (AR0301-13a) has nearly identical MgO–Al_2O_3 to the inferred parent of the Stage 1 eruption (1968–1971; Ryder et al., this issue; Fig. 12), although it is significantly higher in FeO (Fig. 4). Thus, our MI data lend some support to the assumption in Ryder et al. (this issue) that volcanic rocks from the on-going eruption represent liquid compositions. On the other hand, the whole rocks of the on-going eruption possess a pervasive Eu anomaly (Eu/Eu* ~ 1.1), which may derive from plagioclase accumulation or dissolution. Future work may test this proposition for individual samples, by relating modal abundances of crystals to trace element features sensitive to plagiolcase and clinopyroxene accumulation, such as Eu anomalies and Sc excesses.

The population of whole rock samples with <19% Al_2O_3 are comprised mainly of more evolved tephras (<3.5 wt.% MgO), particularly from ET2, 4, and 5 (Fig. 12). These more felsic samples generally contain fewer crystals than the more mafic samples (Melson, 1983), and may more closely approximate liquids. Indeed,

Table 3
Major element analyses of whole rocks and matrix glass

Unit	ET3	ET3	ET3	ET3	ET6	ET6
Sample	AR0301	AR0302	NMNH ET3	NMNH ET3g	NMNH ET6	NMNH ET6g
Type	WR	WR	WR	MG	WR	MG
SiO_2	51.6	50.3	52.4	58.0	51.4	55.3
TiO_2	0.62	0.59	0.58	1.00	0.56	0.78
Al_2O_3	20.6	20.9	20.1	16.8	18.2	18.5
FeO*	8.40	7.93	8.14	8.70	9.09	7.50
MnO	0.16	0.15				
MgO	5.37	5.08	4.74	3.22	6.48	3.34
CaO	10.8	11.2	10.4	6.98	9.9	8.69
Na_2O	2.52	2.56	2.69	3.45	2.02	3.35
K_2O	0.40	0.41	0.42	0.90	0.31	0.57
P_2O_5	0.14	0.12	0.14	0.35	0.12	0.36
Total	100.6	99.3	99.6	99.4	98.1	98.4
Mg#	53.3	53.3	50.9	39.7	56.0	44.3
H_2O^-	2.2%	1.1%				
LOI	0.7%	2.2%				

Major elements for AR0301 and AR0302 acquired by ICP-AES at BU. Total Fe reported as FeO*. LOI = water lost on ignition. NMNH whole rock (WR) and matrix glass (MG) samples reproduced from Melson (1983).

Table 4
Trace element compositions of ET3 melt inclusions and whole rocks

Unit	ET3	ET3	ET3	ET3	ET3			ET3	ET3
Sample name	AR0301–1a	AR0301–2a	AR0301–13a	AR0302–4a	AR0302–5a	BCR–2g		AR0301	AR0302
Type	MI	MI	MI	MI	MI	*Average*	*%RSD*	WR	WR
Li	9.12	11.66	7.95	8.92	4.61	10.085	12%	6.45	5.90
Sc	22.57	21.51	26.97	16.76	17.53	34.54	7%	23.88	21.52
V	260	186	165	134	160	389	6%	204	179
Cr	3.93	16.05	10.68	5.30	13.24	13.79	9%	37.73	33.34
Co	18.2	26.2	36.8	14.9	26.2	39.3	9%	28.4	27.0
Ni	9.56	12.76	26.27	1.02	8.20	10.4	16%	27.97	25.80
Cu	255	470	428	313	69.4	28.5	12%	114.5	99.1
Zn	67.6	105	143	60.1	75.6	152	10%	67.1	60.7
Rb	15.92	11.82	11.84	11.56	6.33	52.5	9%	7.00	6.37
Sr	450	772	682	397	420	348	10%	691	667
Y	26.6	18.8	14.7	19.6	10.1	38.4	10%	13.7	12.1
Zr	60.2	46.6	37.1	72.3	27.2	209	7%	37.5	32.0
Nb	5.90	2.97	3.10	5.30	2.89	14	4%	3.03	2.77
Ba	922	511	397	514	347	670	4%	364	325
La	21.3	12.4	9.45	14.4	7.25	25.5	3%	8.48	7.20
Ce	43.1	29.3	22.3	31.6	15.6	55.1	3%	18.3	15.6
Pr	6.07	4.14	2.45	4.78	1.86	7.10	7%	2.44	2.11
Nd	23.8	15.7	9.70	18.8	9.27	30.0	6%	10.64	9.19
Sm	6.14	3.08	2.61	4.07	2.28	6.90	3%	2.51	2.23
Eu	2.00	1.20	0.808	1.29	0.750	2.10	6%	1.037	0.941
Gd	5.97	3.96	2.32	4.74	2.26	7.50	10%	2.63	2.35
Tb	1.05	0.815	0.354	0.571	0.305	1.16	13%	0.391	0.350
Dy	5.82	3.81	3.28	3.98	2.13	6.99	14%	2.37	2.08
Er	2.79	1.56	1.27	2.09	1.03	3.87	11%	1.30	1.16
Yb	2.62	1.59	1.28	2.20	1.09	3.71	11%	1.29	1.15
Hf	1.83	1.12	0.97	2.44	1.07	5.43	9%	1.06	0.91
Ta	0.310	0.278	0.169	0.570	0.200	0.890	15%	0.161	0.146
Pb	5.95	3.97	3.25	3.39	2.35	11.1	8%	2.14	1.94
Th	1.34	0.570	1.03	1.19	0.450	6.29	11%	0.604	0.499
U	0.594	0.348	0.285	0.567	0.276	1.77	7%	0.237	0.205

Melt inclusion (MI) trace elements acquired by LA-ICP-MS at BU. ^{43}Ca was used as an internal standard (see Table 1). Whole-rock (WR) trace elements acquired by solution ICP-MS. Average RSD of replicate analyses of BCR—2 g was 8%.

liquid line of descent calculations (using the pMELTS algorithm of Ghiorso et al., 2002) demonstrate that these tephras, as well as most of the HAMI, may be derived from the model parent by crystal fractionation of a wet magma (3–4% H_2O) at moderate pressure (~ 3 kbar; Fig. 12). Thus, the HAMI and these tephras, taken together, may record a dominant, wet liquid line of descent for Arenal magmas. The break along the LLD between rocks with increasing Al_2O_3 with decreasing MgO, and those with decreasing Al_2O_3 may mark the late appearance of plagioclase on the high-pH_2O cotectic. The cumulate complements to low-MgO liquids on this liquid line of descent also predict solid compositions very similar to those needed to generate high-MgO, high-Al_2O_3 rocks from the HAMI by crystal accumulation (Fig. 12). If the volcanic rocks of the on-going eruption represent liquid compositions, then they require even greater suppression of plagioclase, due to higher water contents and/or higher pressures of crystallization than the low alumina tephras. This inference is consistent with the high pressures (~ 4 kb) of differentiation also estimated by Ryder et al. (this issue) from their MELTS modeling.

The remaining Arenal magma compositions are the LAMI from ET3 and ET6. These inclusions contain less CO_2 and S than the HAMI of Group A, and so reflect trapping at lower pressures (1.2–0.2 kbar) along decompressing, degassing paths (Figs. 9 and 10). Fig. 7 shows that these inclusions become progressively further out of equilibrium as host Fo contents decrease, reflecting progressively more post-entrapment crystallization and cooling prior to eruption. The low aluminum compositions are consistent with calculated LLD resulting from early plagioclase fractionation at low-pH_2O (~ 0.5 kb, similar to their trapping pressures; Fig. 12). While this low pH_2O

origin of the LAMI seems reasonable given the observations, it is somewhat problematic in that these compositions are never observed in the whole rock population. LAMI do, however, resemble ET3 matrix glass (Fig. 12), supporting the notion that these are residual liquids formed at low pressure, and not caused by some post-entrapment effect unique to the melt inclusions. Thus, LAMI represent residual liquids which may have formed in a shallow mush zone and sampled as glass inclusions or matrix between phenocrysts, and entrained in erupting magmas.

In summary, the melt inclusion data presented here provide baseline parental liquid compositions (HAMI), against which the effects of crystal accumulation (in ET3 whole rocks) and crystal fractionation at high pH_2O (HAMI and low Al_2O_3 tephra) and low pH_2O (LAMI) can be identified. Thus, the broad range of compositions erupted at Arenal may be produced by the complementary process of crystal fractionation and accumulation, from what could be a fairly restricted range of parental liquids. The ET3 HAMI may represent liquids parental to most of Arenal eruptives, and in this way, may relate to the "unseen" compositions referred to in several studies of Arenal (Reagan et al., 1987; Borgia et al., 1988; Beard and Borgia, 1989; Williams-Jones et al., 2001; Streck et al., 2005).

5.2. The H_2O content of Arenal magmas

The new melt inclusion data reported here demonstrate that Arenal magmas are indeed wet, with H_2O contents in ET3 and ET6 melt inclusions ranging from 1.1–3.9 wt.%. The highest water contents are found in the lowest silica melt inclusions (~ 50%, Fig. 2a), trapped at the highest pressures up to 2 kbar (Fig. 9). The lowest water contents are found in the more silicic melt inclusions (~ 57%), trapped at low pressures near 0.2 kbar (Fig. 9). Therefore, as Arenal magmas differentiate, they ascend and degas, driving further crystallization, and finally eruption. On a silica–H_2O diagram (Fig. 2a), the melt inclusions form two arrays, one correlating with higher pressures of entrapment (>1 kbar, as recorded by their H_2O–CO_2 vapor saturation pressures, Fig. 9), and the other, with a greater loss of water per increase in silica, correlating with lower pressures of entrapment (<1 kbar). ET6 inclusions appear to be restricted to the higher P array. Both arrays converge at the low silica end, approaching 4 wt.% H_2O in basaltic melt inclusions.

Thus, our best estimate of the ET3 basaltic magma is 4 wt.% H_2O. These basaltic melt compositions, however, are certainly not primary (i.e., not in equilibrium with mantle peridotite), and a significant history of crystallization and degassing may have preceded entrapment. In fact, if we back-project the H_2O–CO_2 degassing trend for Arenal, it appears to intersect the melt inclusion data for Cerro Negro, with >5% water (Fig. 9). Such high water contents for Arenal, however, are not supported by the H_2O–S degassing path, which is highly curved and asymptotically approaches 4% water at very high sulfur (>3000 ppm), in excess of all sulfur measurements for Cerro Negro (Fig. 10a). In the lack of any other data, we therefore propose 4 wt.% water as an upper limit for Arenal basalts.

In support of this estimate is a calculation based on the Ca–Na exchange hygrometer in Sisson and Grove (1993). Pairing the most mafic ET3 inclusions (>5% MgO; Table 1) with the maximum An measured in the basalt ET3 unit ($An_{92.8–93.1}$) yields a magmatic water content of ~ 4.5 wt.% water (Fig. 2b). Although dependent to a large degree on the plagioclase-melt pairing assumptions, this result is in excellent accord with the maximum water contents measured in ET3 inclusions (3.8–3.9 wt.%). Further work targeting melt inclusions in high An plagioclases (although we found none suitably large enough in our ET3 samples) should test this method, which has enjoyed some success in other studies (Straub and Layne, 2003).

Confirmation of relatively high water contents in the late stages of two of Arenal's eruptive cycles (ET3 and ET6) cause us to reconsider the notion, based on the presence of hornblende in the early blasts of the current eruption, that pH_2O is highest early in the eruptive cycle, and decreases over the course of the eruption (Borgia et al., 1988). Phenocryst data reported by Borgia et al. (1988) in fact indicate the opposite (their Fig. 10b, c). The eruptions leading up to ET3 and ET6, which are late in their respective cycles, show a decrease in modal plagioclase content, with an increase in An content. Because both suppression of plagioclase and high An contents characterize wet magmas (e.g., Sisson and Grove, 1993), it seems likely that pH_2O was actually higher in the later stages of the eruptive cycles, and not the beginning. Hornblende found in enclaves ejected during the early stages of the current eruption in 1968 are not in equilibrium with the host volcanic rocks (Beard and Borgia, 1989) and could have been derived from pre-existing cumulates (Cigolini, 1998).

With a solid understanding of the water variations as a function of Arenal magma evolution, we are now in a position to test predictions of previous studies as to the water content of Arenal magmas. The most direct comparison is with the sum–deficit estimates of ET6 melt inclusions by Melson (1983), since this is the same sample in which we obtained SIMS measurements. The sum–

deficit estimates, which fall between 3.5 and 4.3 wt.% H_2O, are higher than, but generally overlap with, our new measurements (2.8–3.5 wt.% H_2O; Fig. 2a). The more precise SIMS data, however, define a systematic decline of water with increasing silica not observed in the earlier measurements (Fig. 2a). ET6 melt inclusions have fairly low sulfur (<1500 ppm), but otherwise fall on the same S–H_2O degassing trend as ET3. Thus, they may have experienced more degassing, and backtrack to higher H_2O than measured (Fig. 10a). Our best estimate for ET6 (>3.5 wt.% H_2O) is in general accord with the values used by previous workers based on Melson's original work (~ 4 wt.%).

Other petrological predictions of water content for Arenal magmas have been made using volcanic materials from the recent eruption (since 1968), and so are not strictly comparable to our ET3 and ET6 measurements. Nonetheless, the similarity in major and trace element contents of ET3 and recent eruptives invites such a comparison. Several studies used the presence of hornblende, combined with the co-existence of other phases, to argue for water contents from 3–5 wt.% in basaltic andesites (Fig. 2a; Reagan et al., 1987; Beard and Borgia, 1989). This range generally exceeds that measured here in basaltic andesite melt inclusions (<3%), but not that in the basaltic melt inclusions (3–4%). Arenal basaltic melts (i.e. with SiO_2<52 wt.%), however, generally have Na_2O (<3%), too low to stabilize hornblende (Fig. 4c, d; Sisson and Grove, 1993), and so the hornblende-based estimates more reasonably apply to compositions >56% silica (as is appropriate to the Stage 1 lavas of the on-going eruption; Reagan et al., 1987). The wide range of water estimates derived from hornblende stability underscore its use as a blunt tool, which requires independent knowledge of other parameters (e.g. Na, T and P) to use with greater precision. Likewise, the sum–deficit estimates from Anderson (1979) predict values between 0% and 7%, in mostly dacitic melts (Fig. 2a). We find no evidence for water contents higher than 4% in our samples, and so the higher previous estimates either derive from imprecision in the previous techniques, or a fundamental difference in the way that the modern eruption evolves. We note, however, that the estimates of Ryder et al. (2005—this issue) using MELTS (2.5 wt.% H_2O) conform well to our measurements for ET3 basaltic andesite inclusions (Fig. 2a).

In summary, petrologic inferences, and now direct measurements in melt inclusions indicate that Arenal magmas contain up to 4 wt.% H_2O. Although some previous workers estimated much higher H_2O contents for silicic compositions from the recent eruption, these have yet to be confirmed with direct measurements. Olivine is rare in the current eruption, but future work could focus on melt inclusions within other phases (such as high An plagioclases and high Mg# clinopyroxenes), coupled with the use and development of geohygrometers.

5.3. Implications for S fluxes

We can also use the new sulfur data presented here to help reconcile the petrologic vs. spectroscopic estimates of sulfur output at Arenal. Williams-Jones et al. (2001) measured SO_2 fluxes in the volcanic plume at Arenal using correlation spectrometry (COSPEC) in 1982, 1995, and 1996. With these data, they estimate that at least 1.3 Mt (and as much as 3.9 Mt) of SO_2 has been emitted from Arenal between 1968 and 1996. This output is much larger than what they calculated from S concentrations in clinopyroxene- and plagioclase-hosted melt inclusions in recent surge and lava deposits, which averaged 356 ppm. Assuming that the total volume of material extruded from Arenal since 1968 was $\sim 4.6\times10^8$ m^3, their calculation resulted in the emission of SO_2 (ESO_2)=0.41 Mt, a factor of 3–9 times lower than the COSPEC estimate. To account for this discrepancy, they invoke a continuously-replenishing sulfur-rich basaltic magma.

Our sulfur data suggest an alternative explanation, however. The inclusions used by Williams-Jones et al. (2001) were dacitic (Fig. 4), and considerably more degassed than we would predict for the basaltic andesite eruption they were trying to model. Fig. 13 shows sulfur in our mafic to intermediate melt inclusions, compared to their dacitic inclusions. The inclusions as a whole define a sulfur degassing trend as silica in the melt increases. If our pre-historic melt inclusions are representative of the modern magmas, then this trend would predict between 500 and 1500 ppm sulfur in undegassed basaltic andesite magma containing 54–55% SiO_2, like the bulk of the modern eruption (Reagan et al., 1987). This effect alone raises the petrologic estimate by a factor of 1.5–4.3, and into the range of the COSPEC estimates. But Williams-Jones et al. (2001) also assume that their dacitic melt inclusions represent only 50% of the erupted volume, with the other 50% being crystals. If we assume instead that the entire volume of erupted magma was once a bulk basaltic andesite liquid, then the estimates increase by another factor of 2 (3–9), almost precisely within the COSPEC range (Fig. 13).

Quantitative degassing of the observed volume of basaltic andesite liquid erupted from 1968–1996 provides ample sulfur to account for what is measured by COSPEC. In fact, given that parental Arenal basaltic magmas begin with >2000 ppm sulfur, a large surplus of petrologic sulfur must be degassed or lost to other regions of the crust and not contribute to the volcanic plume. This means that SO_2

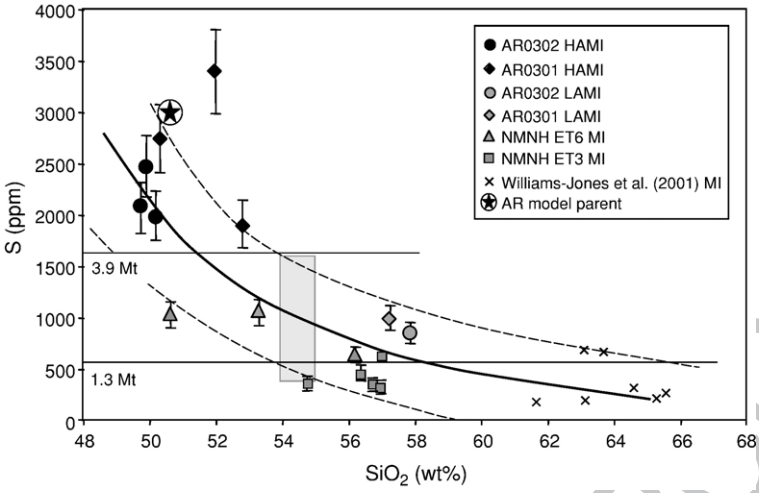

Fig. 13. Variation of sulfur as a function of silica in ET3 and ET6 olivine-hosted melt inclusions (this study, Table 1) and cpx- and plag-hosted melt inclusions from the modern eruption (Williams-Jones et al., 2001). Melt inclusions describe a systematic degassing trend (solid line) for Arenal magmas, from >3000 ppm in parental basalts, to 500–1500 ppm for the basaltic andesites of the modern eruption (shown as a shaded bar), to degassed dacites (<700 ppm). Modern eruption estimate (shaded bar) derives from restricted silica range of 54–55% observed for most of the modern eruption (Reagan et al., 1987), and the full width of the sulfur degassing trend (curves fit by eye). This range is virtually identical to that required to explain the COSPEC-derived sulfur outputs at the Arenal plume from 1968–1996 (1.3–3.9 Mt; Williams-Jones et al., 2001). Sulfur outputs calculated using parameters in Williams-Jones et al. (2001), but assuming phi(melt)=1.0 instead of 0.5, or that the volume of erupted material is a bulk liquid of the concentration given by the lines. Sulfur error bars as in Fig. 10.

fluxes measured in volcanic plumes may grossly underestimate basaltic fluxes.

5.4. Implications for slab proxies

A final implication of our results is for the cycling of water and other tracers from the downgoing plate to the mantle source beneath Arenal. Because water measurements in arc magmas are rare, existing literature has relied on various proxies, such as boron (Leeman et al., 1994) and Ba/La (Walker et al., 1995), based on their presumed "fluid-mobile" behavior. Now that we have both an estimate of magmatic H_2O and trace element data on a set of melt inclusions, we can evaluate the accuracy of slab-derived fluid proxies such as Ba/La. It is first important to note the similarity in Ba/La between our melt inclusions and Arenal whole rocks, particularly those from ET3 (Table 4, Fig. 5b). Moreover, the relative constancy in Ba/La (41–43) in ET3 sample AR0301 (Table 4), over a large range in silica (50–57%), provides evidence against crustal contamination, as has been proposed by Cigolini (1998), based on the presence of crustal xenoliths in the early phase of the recent eruption. These observations support an uncontaminated, common lineage between the parent magma of the melt inclusions and the ET3 whole rocks.

The water contents of Arenal basaltic melt inclusions (~ 4 wt.%) are less than those from Fuego (4–5 wt.%; Sisson and Layne, 1993; Roggensack, 2001b) and Cerro Negro (5–6 wt.%; Roggensack et al., 1997) but greater than those from Irazú (~ 3 wt.%; Benjamin et al., 2004), and this is the same sense of variation as Ba/La (e.g., from >100 for Cerro Negro, and <25 for Irazú). Before comparing these variations in detail, however, water contents must be corrected for differences in the extent of differentiation with respect to primary magmas. If we add olivine to the melt inclusion compositions until they are in equilibrium with mantle olivine (Fo_{90}), there is much less difference in primary water contents (H_2O_{Fo90}) along-arc (Fig. 14). Cerro Negro is still the wettest (avg. H_2O_{Fo90} ~ 3.6 wt.%) and Irazú the driest (avg. H_2O_{Fo90} ~2.4 wt.%, higher only than Guatemalan behind-the-front (BVF) volcanoes; Fig. 14), but the total range is now only a factor of 1.5. Within this restricted range, the primary H_2O_{Fo90} contents do correlate with Ba/La, and so there is some basis for using Ba/La as a water proxy. Moreover, within ET3 samples from Arenal, AR0302 appears to have slightly higher water (also at constant S; Fig. 10a), as well as higher Ba/La (Fig. 14), so these parameters may correlate at a fine scale.

The variation of Ba/La with water, however, is not simply related to progressive addition of a H_2O-rich and Ba/La-rich component to a MORB or OIB mantle. All the Central American magmas have water contents that are significantly higher than MORB or OIB, despite the fact that Ba/La approaches OIB values in Irazú. In fact, these results are counter to previous notions that Costa Rican

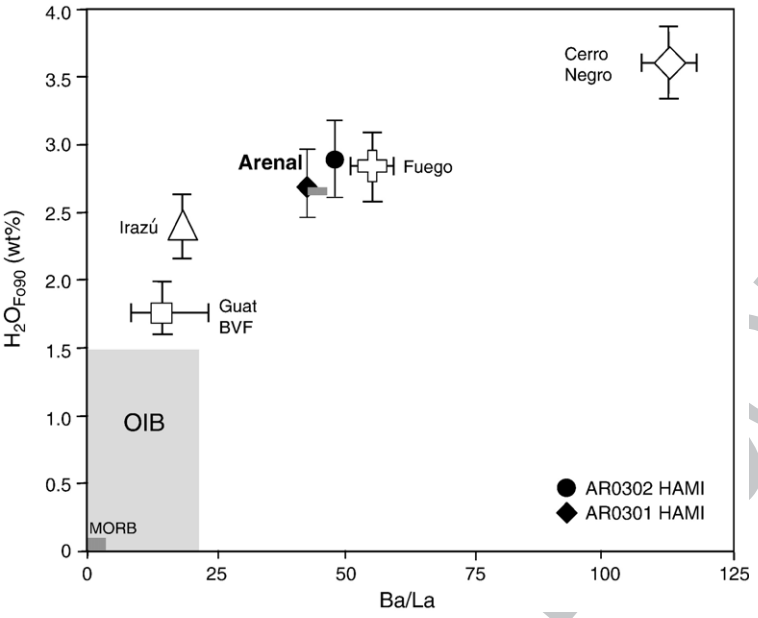

Fig. 14. Ba/La versus H_2O in Arenal, Irazú, Cerro Negro, Fuego, and Guatemalan BVF melt inclusions, calculated to be in equilibrium with the mantle (Fo_{90}), assuming $K_D^{Mg/Fe}=0.3$ and that 20% of iron is Fe^{3+}. Open symbols are the averages for each volcano (error bars enclose the total range), and Arenal ET3 points are plotted individually (error bars indicate 10% rsd). Gray bar is possible range for ET6, based on the highest-H_2O MI and the range in Ba/La for the unit (Bolge et al., 2005). Guatemalan BVF data from Walker et al. (2003). Irazú data is unpublished (Benjamin et al.). Other data sources as in Fig. 10, and exclude those that may have degassed significant water (i.e. with S < 1000 ppm, and CO_2 < 200 ppm). Maximum H_2O in OIB comes from data in Dixon et al. (2002), assuming average OIB Ce of 80 ppm (Sun and McDonough, 1989) and the high end of OIB range for H_2O/Ce of 200 (also from Dixon et al., 2002). MORB from Salters and Stracke (2004) assuming mean mantle melt fraction of 10%.

volcanics derive largely from an enriched OIB mantle with a weak or absent subduction component (e.g. Carr, 1984; Herrstrom et al., 1995; Patino et al., 2000). Arenal MI with >3 wt.% H_2O have H_2O/Ce of 1000–2300 (Table 4), roughly an order of magnitude higher than that in the MORB-OIB mantle (H_2O/Ce = 100–250; Dixon et al., 2002). Even without subtracting the Ce contributions from the slab, this requires up to an order of magnitude higher H_2O in the mantle source to Arenal than MORB-OIB mantle.

Even more noteworthy are the high Cl contents in Costa Rican magmas (Arenal and Irazú), higher than those in Nicaraguan magmas. Thus for some slab tracers (Cl), Costa Rican volcanoes actually bear a dominant signal. The ratio of Cl to H_2O also varies systematically from volcano to volcano, with the lowest ratios at Cerro Negro, and the highest at Irazú (Fig. 15). If we convert these to equivalent salinities (following Kent et al., 2002), then the Cerro Negro fluid is similar to seawater salinity (~ 3%), while the Irazú fluid is five times more saline. Thus, questions as to the mantle composition aside, different slab components appear to feed the different volcanoes along the Central American arc, from a water-rich, low salinity, high Ba/La fluid at Cerro Negro, to a fluid with the opposite characteristics at Irazú, and Arenal falling in between.

What is the source of these different slab components that vary along the arc? There are three key parameters that vary along-strike of the trench that may contribute to differences in the slab component. First is the extent of hydration of the down-going plate, which appears to be greater off Nicaragua than Costa Rica. This is based on the extent of outer rise faulting (Ranero et al., 2003), the seismic velocity of the slab waveguide (Abers et al., 2003), and low-$\delta^{18}O$ values in wet Nicaraguan lavas which may be a result of serpentine-derived fluids (Eiler et al., 2005). Second is the greater contribution to Nicaragua volcanoes of the uppermost pelagic sediments, which contain high ^{10}Be and Ba/La (Patino et al., 2000), than to Costa Rica volcanoes (Tera et al., 1986), where the uppermost sediment appears to be underplated (Morris et al., 2002). Third is the appearance of Galapagos-derived igneous and volcaniclastic material to the south at the Cocos Ridge and nearby seamounts (Werner et al., 1999; Hoernle et al., 2000), which contribute material to central Costa Rica (Arenal to Irazú) with low Ba/La (like OIB) and presumably high water and Cl (seawater-altered volcaniclastic sediments and igneous rocks). As a result of

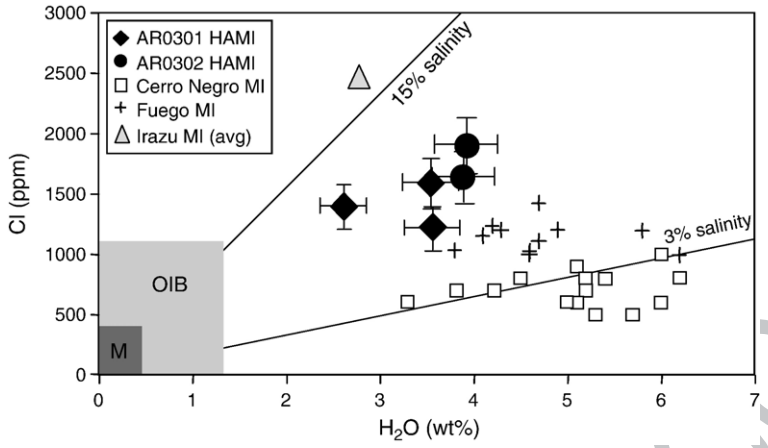

Fig. 15. Water and chlorine in Arenal MI's, compared to other Central American MI's. Lines of constant Cl/H_2O and calculated salinities (after Kent et al., 2002). Melt inclusion data sources as in Figs. 10 and 14, and were screened for degassing as in Fig. 14.

these effects, the high water, Ba/La and ^{10}Be of Nicaragua may relate to the greater hydration of the crust and efficient subduction of pelagic sediments, while the lower water, ^{10}Be and Ba/La of Costa Rica relates to loss of the pelagic sediment and gain of OIB volcanic material to the subduction zone. With multiple sources potentially contributing along the arc (serpentine, altered oceanic crust, pelagic sediments, and volcaniclastic material), a simple H_2O proxy seems unlikely. Clearly the above hypotheses, as well as the basis for the Ba/La proxy, require testing with more measurements of the volatile content of Central American volcanoes.

6. Conclusions

With a relatively small number of well-chosen MI, we are able to determine an elusive but fundamental parameter in Arenal magmas: the volatile content of the basaltic liquid parental to Arenal eruptives. We have made here the first direct water measurements of Arenal melts, and related them to the magmatic evolution and subducted sources beneath Arenal volcano. Below are the main results and conclusions of this work:

1. Olivine-hosted melt inclusions from prehistoric ET3 tephra include high-aluminum basaltic liquids hosted in $Fo_{76–79}$ olivines and contain up to 4 wt.% H_2O, 300 ppm CO_2, 3000 ppm S, 1500 ppm Cl and 300 ppm F. Unlike some melt inclusions in the literature, these are close to equilibrium with their host olivines, and reflect trace element compositions similar to that of the host magma. The population of olivine phenocrysts in ET3 tephra could have formed during crystallization of the host magma, and do not appear to be exotic. Thus the volatile and major element contents of the ET3 melt inclusions presumably reflect that of the ET3 parental liquids, and we present here an Arenal "model parent" based on the most mafic and least degassed MI compositions (Table 2).
2. The high sulfur concentrations (>2500 ppm) of the least degassed ET3 inclusions are in excess of what would be expected for sulfide-saturated melts from the mantle. This is consistent with 58–84% of the total sulfur speciated as sulfate, and high fO_2 in Arenal mafic magmas (NNO+0.5 to+1.1).
3. H_2O, CO_2 and S covary in a manner consistent with degassing of a vapor phase, from 2 kbar to 0.2 kbar. Cl and F, on the other hand, behave like, and correlate with, other incompatible trace elements (e.g. U). These relationships are expected from the known solubility of volatile species in silicate melts. F/Cl varies by more than a factor of 2 between different samples of ET3.
4. Degassing and ascent, as estimated from vapor saturation relationships, correlate with measures of magma differentiation, such as Si, K and Fo. Therefore polybaric crystal fractionation, with decreasing pH_2O, is one driver of magma evolution at Arenal. The most degassed melts, with H_2O–CO_2 vapor saturation pressures of <1.2 kbar, also have unusual, low-Al compositions that are unlike any erupted lava or tephra from Arenal. They are similar, however, to matrix glass compositions, and appear to be residual liquids formed and trapped at shallow depths in the magmatic plumbing system.
5. The high alumina melt inclusions are better candidates for Arenal liquids than ET3 whole rocks, most of which have suffered as much as 30–40% crystal accumulation of plagioclase and clinopyroxene. A few melt inclusions

from ET3 olivines are similar to parental and derivative melts inferred for the on-going eruption by Ryder et al. (this issue). Some Arenal volcanic rocks and glasses lie on model liquid lines of descent derived from the model parent, at different pressures (0.5–3 kb) and H_2O (0.5–3.5 wt.%). In the case of Arenal, melt inclusions provide not just volatile information, but otherwise unmeasured and unseen magmatic liquid compositions.

6. Using ET3 and ET6 melt inclusions as analogs, quantitative degassing of the observed volume of basaltic andesite liquid erupted in 1968–1996 could have provided ample sulfur to account for that measured by COSPEC.
7. Based on H_2O–S degassing systematics, 4% H_2O is the best maximum estimate for undegassed mafic ET3 magmas. This estimate is somewhat lower than the earlier estimates of Melson (1983) by sum–deficit for ET6, and present data define well the polybaric degassing paths from basalt to andesite. The similarity between ET3 and ET6 tephra and recent eruptives suggest that 4% water may be typical of modern mafic precursors as well.
8. The high water and Cl contents of Arenal magmas were not predicted by other geochemical tracers of the slab (^{10}Be, Ba/La, B/La, U/Th), which show a weak subduction signal. For example, Ba/La in Arenal is almost 3 times lower than for Cerro Negro in Nicaragua, while calculated primary water contents are only 1.3 times lower. Existing data from four Central American volcanoes (Irazú, Arenal, Fuego and Cerro Negro) show a positive relationship between H_2O and Ba/La, but with a high H_2O_{Fo90} intercept, suggesting sources of water in the subduction zone from low-Ba/La materials. This makes sense given that pelagic sediments will contribute high Ba/La, but other hydrous sources (e.g. altered oceanic crust, serpentinites, volcaniclastic sediments) may not.

7. Uncited references

Bolge et al., this issue
Plank and Langmuir, 1998

Acknowledgements

We thank Geoff Abers, Guillermo Alvarado, and Jim Gill for their valuable comments and support, and Louise Bolge for the conversation, perspective, and data. Detailed and helpful reviews from Mark Reagan, Kurt Roggensack and an anonymous reviewer greatly improved the text and presentation of the data. Thanks to Nilanjan Chatterjee, Charles Mandeville, and Mindy Zimmer for their analytical help, and to ICE and the MARGINS program for the continued sponsorship of our endeavors. This work was made possible by the NSF OCE-0001897 and OCE-0203650 (PI, Plank).

Appendix A

Table A1
Olivine compositions

Sample	Lab$_{EMP}$	SiO_2	TiO_2	Al_2O_3	FeO	MnO	MgO	CaO	Total	Fo_{adj}	Fo_{core}	Sc	V	Cr	Co	Ni	Cu	Zn	Section
Inclusion-bearing olivines																			
AR0301–1	M	38.1	0.01	0.02	21.5	0.33	38.7	0.09	98.7	76	78	6.24	3.10	3.09	168	542	5.25	95.9	Core
AR0301–2	A	38.3	0.01	0.01	22.7	0.42	39.0	0.12	100.5	75	81	4.51	3.35	10.93	156	777	8.48	128	Core
AR0301–3	A	37.2	0.04	0.02	20.0	0.28	41.3	0.13	98.9	79									
AR0301–13	A	38.0	0.02	0.39	20.2	0.36	38.6	0.07	97.7	77	78	8.75	3.56	30.12	176	937	8.52	112	Core
AR0302–1a	M	38.5	0.02	0.04	22.4	0.26	39.2	0.09	100.5	76									
AR0302–1b	M	38.4	0.01	0.12	23.3	0.32	38.3	0.12	100.5	75									
AR0302–3	A	37.5	0.01	0.00	21.3	0.35	40.0	0.12	99.3	77									
AR0302–4	M	38.1	0.01	0.00	21.8	0.32	39.0	0.10	99.3	76	76	1.68	3.89	–	162	783	8.36	94.6	Core
AR0302–5	A	37.1	0.00	0.03	23.2	0.33	37.9	0.10	98.7	74	81	5.89	2.11	14.22	166	326	5.81	134	Core
NMNH ET3a-ol	A	36.7	0.02	0.03	24.2	0.50	37.2	0.11	98.7	73									
NMNH ET3b-ol	A	36.4	0.01	0.00	24.5	0.46	36.6	0.14	98.1	73									
NMNH ET3c-ol	M	37.4	0.02	0.00	24.6	0.50	36.7	0.17	99.3	73									
NMNH ET3c-ol	A (rep)	37.2	0.04	0.00	25.5	0.48	36.8	0.12	100.1	72									
NMNH	A	37.9	0.01	0.00	22.7	0.42	37.5	0.11	98.6	75									

Table A1 (*continued*)

Sample	Lab_{EMP}	SiO_2	TiO_2	Al_2O_3	FeO	MnO	MgO	CaO	Total	Fo_{adj}	Fo_{core}	Sc	V	Cr	Co	Ni	Cu	Zn	Section
ET6a-ol																			
NMNH	A	37.1	0.00	0.01	22.4	0.35	37.6	0.14	97.6	75									
ET6b-ol																			
NMNH	A	37.8	0.03	0.00	21.3	0.43	38.7	0.10	98.3	76									
ET6c-ol																			
NMNH	A	46.6	0.46	6.96	6.81	0.17	14.3	21.72	97.0	79									
ET6d-ol																			
NMNH	A (rep)	48.9	0.57	3.03	10.8	0.41	14.1	18.81	96.5	70									
ET6d-ol																			
Non-inclusion-bearing olivines																			
AR0301-10	A	38.1	0.01	0.00	21.6	0.27	39.1	0.07	99.1	76	79	9.55	2.96	–	154	691	6.92	99	Core
AR0301-11											81	9.34	2.94	5.04	158	796	5.15	94	core
AR0301–12	A	38.6	0.02	0.03	17.8	0.23	41.8	0.08	98.6	81	81	8.90	3.17	–	183	1144	5.24	88	R side
AR0301–14	A	38.4	0.02	0.03	21.1	0.32	38.1	0.10	98.1	76	80	8.14	2.98	34.33	158	937	7.21	90	Core
AR0301–15	A	39.2	0.00	0.00	18.2	0.33	41.0	0.10	98.8	80	80	10.73	3.35	25.28	172	1039	6.92	96	Core
AR0301–16											77	10.84	3.08	104.69	178	662	10.2	129	Core
NMNH	A	36.3	0.00	0.00	24.3	0.53	36.6	0.13	97.8	73									
ET3g–ol																			
NMNH	A	37.3	0.00	0.00	22.6	0.38	37.5	0.12	97.9	75									
ET3h–ol																			
San Carlos					9.91	0.153	47.6				90	6.22	3.01	121.4	126	2900	6.55	46.8	
olivine																			
SD					*0.4*	*0.002*	*1.7*				*0.4*	*1.0*	*0.2*	*51.4*	*6.1*	*47.3*	*4.5*	*3.9*	
Rsd					*3.9%*	*1.3%*	*3.5%*				*0.39%*	*16%*	*7.4%*	*42%*	*4.8%*	*2.2%*	*68%*	*8.3%*	

Major element compositions determined at single points by EMP at either MIT (M) or AMNH (A). Trace element compositions determined by LA-ICP-MS at BU, with the laser in line scan mode (Fig. 3; see Section 3.3 for conditions). Section of the line scan reduced for trace element data as indicated. San Carlos olivine data are averages of 3 replicate analyses across 3 analytical sessions. Isotopes monitored during LA-ICP-MS analyses were ^{58}Fe, ^{55}Mn,^{25}Mg, ^{45}Sc, ^{51}V, ^{52}Cr, ^{59}Co, ^{60}Ni, ^{65}Cu, ^{66}Zn. Fo_{adj} indicates an analysis of the olivine directly adjacent to the MI, via EMP. Fo_{core} indicates an anlysis of the olivine in its compositional core, via LA-ICP-MS.

References

Abers, G.A., Plank, T., Hacker, B.R., 2003. The wet Nicaraguan slab. Geophysical Research Letters 30 (2) doi:10.1029/2002GL015649.

Anderson, A.T., 1979. Water in some hypersthenic magmas. Journal of Geology 87, 509–531.

Asimow, P.D., Dixon, J.E., Langmuir, C.H., 2004. A hydrous melting and fractionation model for mid-ocean ridge basalts: application to the mid-Atlantic ridge near the Azores. Geochemistry, Geophysics, Geosystems 5 (1), doi:10.1029/2003GC000568.

Beard, J.S., Borgia, A., 1989. Temporal variation of mineralogy and petrology in cognate gabbroic enclaves at Arenal volcano, Costa Rica. Contributions to Mineralogy and Petrology 103, 110–122.

Benjamin, E.R., Plank, T., Hauri, E.H., Kelley, K.A., Wade, J.A., Alvarado, G.E., 2004. Water content of a hypothetically dry magma: the 1723 and 1963–65 eruptions of Irazú volcano, Costa Rica. Eos, Transactions AGU 85 (17) (Jt. Assem. Suppl., Abstract V54B-02).

Bolge, L.L., Carr, M.J., Feigenson, M.D., Borgia, A., 2004. The geochemistry and magmatic evolution of explosive tephra 3 and 4 from Arenal Volcano, Costa Rica. In: Soto, G.J., Alvarado, G.E. (Eds.), Revista Geológica de América Central. Universidad de Costa Rica.

Bolge, L.L., Carr, M.J., Feigenson, M.D., Alvarado, G.E., this issue. Geochemical stratigraphy and magmatic evolution at Arenal volcano, Costa Rica. Journal of Volcanology and Geothermal Research.

Borgia, A., Poore, C., Carr, M.J., Melson, W.G., Alvarado, G.E., 1988. Structural, stratigraphic, and petrologic aspects of the Arenal–Chato volcanic system, Costa Rica: evolution of a young stratovolcanic complex. Bulletin of Volcanology 50, 86–105.

Carmichael, I.S.E., 1991. The redox states of basic and silicic magmas: a reflection of their source regions? Contributions to Mineralogy and Petrology 106, 129–141.

Carr, M.J., 1984. Symmetrical and segmented variation of physical and geochemical characteristics of the Central American volcanic front. Journal of Volcanology and Geothermal Research 20, 231–252.

Carr, M.J., Feigenson, M.D., Patino, L.C., Walker, J.A., 2003. Volcanism and geochemistry in Central America: progress and problems. Inside the Subduction Factory, Geophysical Monograph, vol. 138. The American Geophysical Union, pp. 153–179.

Carroll, M.R., Rutherford, M.J., 1988. Sulfur speciation in hydrous experimental glasses of varying oxidation state: results from measured wavelength shifts of sulfur X-rays. American Mineralogist 73, 845–849.

Cervantes, P., Wallace, P.J., 2003. Magma degassing and basaltic eruption styles; a case study of approximately 2000 year BP Xitle Volcano in central Mexico. Journal of Volcanology and Geothermal Research 120 (3–4), 249–270.

Cigolini, C., 1998. Intracrustal origin of Arenal basaltic andesite in the light of solid–melt interactions and related compositional buffering. Journal of Volcanology and Geothermal Research 86, 277–310.

Danyushevsky, L.V., Leslie, R.A., Crawford, A.J., Durance, P., 2004. Melt inclusions in primitive olivine phenocrysts: the role of localized reaction processes in the origin of anomalous compositions. Journal of Petrology 45 (12), 2531–2553.

Devine, J.D., Gardner, J.E., Brack, H.P., Layne, G.D., Rutherford, M.J., 1995. Comparison of microanalytical methods for estimating H_2O contents of silicic volcanic glasses. American Mineralogist 80 (3–4), 319–328.

Dixon, J.E., Leist, L., Langmuir, C., Schilling, J.-G., 2002. Recycled dehydratrated lithosphere observed in plume-influenced mid-ocean-ridge basalt. Nature 420, 385–389.

Eiler, J.M., Carr, M.J., Reagan, M., Stolper, E., 2005. Oxygen isotope constraints on the sources of Central American arc lavas. Geochemistry, Geophysics, Geosystems 6 (7), doi:10.1029/2004GC000804.

Ghigliotti, M., Frullani, A., Alvarado, G.E., Soto, G.J., 1993. Distribución areal y caracteristicas de los depositos de tefra màs recientes (1080–1968 dC) del Volcán Arenal. Boletín Observatorio Vulcanológico del Arenal 4 (8), 11–33.

Ghiorso, M.S., Sack, R.O., 1995. Chemical mass transfer in magmatic processes. IV. A revised and internally consistent thermodynamic model for the interpolation and extrapolation of liquid-solid-equilibria in magmatic systems at elevated temperatures and pressures. Contributions to Mineralogy and Petrology 119, 197–212.

Ghiorso, M.S., Hirschmann, M.M., Reiners, P.W., Kress III, V.C., 2002. The pMELTS: a revision of MELTS for improved calculation of phase relations and major element partitioning related to partial melting of the mantle to 3 GPa. Geochemistry, Geophysics, Geosystems 3 (5), doi:10.1029/2001GC000217.

Hauri, E., 2002. SIMS analysis of volatiles in silicate glasses. 2: isotopes and abundances in Hawaiian melt inclusions. Chemical Geology 183, 115–141.

Hauri, E., Wang, J., Dixon, J.E., King, P.L., Mandeville, C., Newman, S., 2002. SIMS analysis of volatiles in silicate glasses 1. Calibration, matrix effects and comparisons with FTIR. Chemical Geology 183, 99–114.

Herrstrom, E.A., Reagan, M.K., Morris, J.D., 1995. Variations in lava composition associated with flow of asthenosphere beneath southern Central America. Geology 23 (7), 617–620.

Hoernle, K., Werner, R., Phipps Morgan, J., Garbe-Schonberg, D., Bryce, J., Mrazek, J., 2000. Existence of complex spatial zonation in the Galapagos plume for at least 14 m.y. Geology 28 (5), 435–438.

Kelley, K.A., Plank, T., Ludden, J., Staudigel, H., 2003. Composition of altered oceanic crust at ODP Sites 801 and 1149. Geochemistry, Geophysics, Geosystems 4 (6), doi:10.1029/2002GC000435.

Kent, A.J.R., Peate, D.W., Newman, S., Stolper, E.M., Pearce, J., 2002. Chlorine in submarine glasses from the Lau Basin: seawater contamination and constraints on the composition of slab-derived fluids. Earth and Planetary Science Letters 202, 361–377.

Leeman, W.P., Carr, M.J., Morris, J.D., 1994. Boron geochemistry of the Central America volcanic arc: constraints on the genesis of subduction-related magmas. Geochimica et Cosmochimica Acta 58, 149–168.

Luhr, J.F., 2001. Glass inclusions and melt volatile contents at Paricutin Volcano, Mexico. Contributions to Mineralogy and Petrology, doi:10.1007/s004100100293.

Mandeville, C.W., Webster, J.D. Tappen, C. Taylor, B.E. Timbal, A. Sasaki, A. Hauri, E. Bacon, C.R., in review. Stable isotope and petrologic evidence for open-system degassing during the climactic and pre-climactic eruptions of Mt. Mazama, Crater Lake, Oregon. Geochimica et Cosmochimica Acta.

Melson, W.G., 1983. Alternation between acidic and basic magmas in major explosive eruptions of Arenal volcano, Costa Rica. Boletin de Volcanologia, Universidad Nacional, Costa Rica, vol. 14, pp. 65–74.

Melson, W.G., Saenz, R., 1973. Volume, energy, and cyclicty of eruptions of Arenal volcano, Costa Rica. Bulletin of Volcanology 37, 416–437.

Metrich, N., Clocchiatti, R., 1996. Sulfur abundance and its speciation in oxidized alkaline melts. Geochimica et Cosmochimica Acta 60 (21), 4151–4160.

Morris, J., Valentine, R., Harrison, T., 2002. ^{10}Be imaging of sediment accretion and subduction along the northeast Japan and Costa Rica convergent margins. Geology 30 (1), 59–62.

Newman, S., Lowenstern, J.B., 2002. VolatileCalc: a silicate melt H_2O–CO_2 solution model written in visual basic for excel. Computers and Geosciences 28, 597–604.

Patino, L.C., Carr, M.J., Feigenson, M.D., 2000. Local and regional variations in Central American arc lavas controlled by variations in subducted sediment input. Contributions to Mineralogy and Petrology 138, 265–283.

Plank, T., Langmuir, C.H., 1998. The chemical composition of subducting sediment and its consequences for the crust and mantle. Chemical Geology 145, 325–394.

Ranero, C.R., Phipps Morgan, J., McIntosh, K., Reichert, C., 2003. Bending-related faulting and mantle serpentinization at the Middle America trench. Nature 425, 367–373.

Reagan, M.K., Gill, J.B., Malavassi, E., Garcia, M.O., 1987. Changes in magma composition at Arenal volcano, Costa Rica, 1968–1985: Real-time monitoring of open-system differentiation. Bulletin of Volcanology 49, 415–434.

Reagan, M.K., Tepley, III, F.J., Gill, J.B. Wortel, M. Garrison, J., this issue. Timescales of degassing and crystallization implied by ^{210}Po-^{210}Pb- ^{226}Ra disequilibrium for andesitic lavas erupted from Arenal volcano.

Roggensack, K., 2001a. Sizing up crystals and their melt inclusions: a new approach to crystallization studies. Earth and Planetary Science Letters 187, 221–237.

Roggensack, K., 2001b. Unraveling the 1974 eruption of Fuego volcano (Guatemala) with small crystals and their young melt inclusions. Geology 29 (10), 911–914.

Roggensack, K., Hervig, R.L., McKnight, S.B., Williams, S.L., 1997. Explosive basaltic volcanism from Cerro Negro volcano: influence of volatiles on eruptive style. Science 277, 1639–1642.

Ryder, C.H., Gill, J.B., Tepley III, F., Ramos, F. Reagan, M.K., this issue. Closed to open system differentiation at Arenal Volcano (1968–2003).

Salters, V.J.M., Stracke, A., 2004. Composition of the depleted mantle. Geochemistry, Geophysics, Geosystems 5 (5), doi:10.1029/2003GC000597.

Sisson, T.W., Grove, T.L., 1993. Experimental investigations of the role of H_2O in calc-alkaline differentiation and subduction zone magmatism. Contributions to Mineralogy and Petrology 113, 143–166.

Sisson, T.W., Layne, G.D., 1993. H_2O in basaltic andesite glass inclusions from four subduction-related volcanoes. Earth and Planetary Science Letters 117, 619–635.

Soto, G.J., Alvarado, G.E., this issue. Eruptive history of Arenal volcano, Costa Rica, 7 ka to present. Journal of Volcanology and Geothermal Research.

Soto, G.J., Alvarado, G.E., Ghigliotti, M., 1998. El registro eruptivo del Arenal en el lapso 3000–7000 años antes del presente y nuevas deducciones sobre la edad del volcán. Boletín OSIVAM 9 (17–18), 19–49.

Soto, G.J., Alvarado, G.E., Bonilla, J., Madrigal, J., Mata, A., Ramirez, R., Rojas, L., Salazar, J., Tristán, E., Villegas, A., 2000. Las facies proximales de la gran erupción piroclástica basáltica ET-3 del volcán Arenal. Boletín OSIVAM 12 (23–24), 54–63.

Stolper, E., Newman, S., 1994. The role of water in the petrogenesis of Mariana trough magmas. Earth and Planetary Science Letters 121, 293–325.

Straub, S.M., Layne, G.D., 2003. The systematics of chlorine, fluorine, and water in Izu arc front volcanic rocks: implications for volatile recycling in subduction zones. Geochimica et Cosmochimica Acta 67 (21), 4179–4203.

Streck, M.J., Dungan, M.A., Malavassi, E., Reagan, M.K., Bussy, F., 2002. The role of basalt replenishment in the generation of basaltic andesites of the ongoing activity at Arenal volcano, Costa Rica: evidence from clinopyroxene and spinel. Bulletin of Volcanology 64, 316–327.

Streck, M.J., Dungan, M.A., Bussy, F., Malavassi, E., 2005. Mineral inventory of continuously eruption basaltic andesites at Arenal volcano, Costa Rica: implications for interpreting monotonous, crystal-rich, mafic arc stratigraphies. Journal of Volcanology and Geothermal Research 140, 133–155.

Sun, S., McDonough, W.F., 1989. Chemical and isotopic systematics of oceanic basalts: implications for mantle composition and processes. In: Saunders, A.D., Norrey, M.J. (Eds.), Magmatism in the Ocean Basins. Geological Society, London, Special Publications, vol. 42, pp. 313–345.

Tera, F., Brown, L.D., Morris, J.D., Sacks, S.I., Klein, J., Middleton, R., 1986. Sediment incorporation in island-arc magmas: inferences from ^{10}Be. Geochimica et Cosmochimica Acta 50, 535–550.

Walker, J.A., Carr, M.J., Patino, L.C., Johnson, C.M., Feigenson, M.D., Ward, R.L., 1995. Abrupt change in magma generation processes across the Central American arc in southeastern Guatemala: flux-dominated melting near the base of the wedge to decompression melting near the top of the wedge. Contributions to Mineralogy and Petrology 120, 378–390.

Walker, J.A., Roggensack, K., Patino, L.C., Cameron, B.I., Matias, O., 2003. The water and trace element contents of melt inclusions across an active subduction zone. Contributions to Mineralogy and Petrology 146 (1), 62–77.

Wallace, P.J., 2005. Volatiles in subduction zone magmas: concentrations and fluxes based on melt inclusion and volcanic gas data. Journal of Volcanology and Geothermal Research 140, 217–240.

Wallace, P.J., Carmichael, I.S.E., 1992. Sulfur in basaltic magmas. Geochimica et Cosmochimica Acta 56, 1863–1874.

Wallace, P.J., Carmichael, I.S.E., 1994. S speciation in submarine basaltic glasses as determined by measurements of SKa X-ray wavelength shifts. American Mineralogist 79, 161–167.

Webster, J.D., 2004. The exsolution of magmatic hydrosaline chloride liquids. Chemical Geology 210 (1–4), 33–48.

Webster, J.D., 2005. Consequences of exsolution of H_2O-, CO_2-, SO_2-, Cl-bearing volatile phases on the physical and chemical properties of magma. Goldschmidt Conference Abstracts, vol. A151.

Werner, R., Hoernle, K., van de Bogaard, P., Ranero, C., von Huene, R., 1999. Drowned 14-m.y.-old Galapagos archipelago off the coast of Costa Rica: implications for tectonic and evolutionary models. Geology 27 (6), 499–502.

Williams-Jones, G., Stix, J., Heiligmann, M., Barquero, J., Fernandez, E., Gonzalez, E.D., 2001. A model of degassing and seismicity at Arenal Volcano, Costa Rica. Journal of Volcanology and Geothermal Research 108, 121–139.